Very few reports describe comparisons of multiple parameters, including the relative cerebral blood flow (rCBF)-measured PASL sequence on 3T MR imaging, and glioma grading. Immunohistologically, the Ki-67 labeling index on histologic examinations is known to correlate with malignancy, and it also functions as a marker of proliferation in gliomas.[19] According to the previous literature, this index is correlated with various advanced MR imaging parameters.[8,20,21]

In this study, we performed a comparative review of multiple parameters obtained with pulse sequences evaluated by using 3T MR imaging and glioma grading in newly diagnosed patients with glioma. Our purpose was to evaluate whether the parameters provide useful, complementary information and whether this combination of parameters shows the best performance for grading cerebral gliomas. The results of the present study are clinically valuable for evaluating sensitivity, specificity, positive predictive value (PPV), and negative predictive value (NPV) and determining the threshold values by analyzing receiver operating characteristic (ROC) curves. Under the same conditions, we evaluated the correlations between various MR imaging parameters and the proliferation marker, the Ki-67 labeling index.

MATERIALS AND METHODS

Patients

Thirty-two patients ranging in age from 16 to 82 years with newly diagnosed supratentorial glioma, to avoid confounding findings related to posttherapeutic effects, were entered into this study. All patients underwent PASL, DTI, and MR spectroscopy studies by using 3T MR imaging. We reviewed all PASL, FA, ADC, and MR spectroscopy studies of supratentorial cerebral gliomas performed between March 2010 and October 2012. No patients had a clinical history of previous surgery, chemotherapy, or radiation therapy.

The histologic analysis was performed, according to the World Health Organization brain tumor classification revised in 2007, of tissue samples obtained at the time of either surgical resection or image-guided biopsies.[1]

All patients provided their informed consent to participate in this study, which was conducted in accordance with the ethical principles of the Declaration of Helsinki. The study protocol was approved by the Ethics Committee of the Oita University Faculty of Medicine.

MR Imaging Protocol

Conventional MR imaging included T1-weighted spin-echo, T2-weighted fast spin-echo, fluid-attenuated inversion recovery, and contrast-enhanced T1-weighted axial imaging (0.1-mmol/kg meglumine gadoterate, Magnescope; Guerbet Japan, Tokyo, Japan) performed at a field strength of 1.5T. After 2–5 days, we performed the advanced MR imaging examination. All participating patients underwent an advanced MR imaging protocol that included PASL, DTI, MR spectroscopy, and SWI by using a superconducting magnet at a field strength of 3T (Magnetom Verio; Siemens, Erlangen, Germany). T1-weighted structural images were acquired with a 3D MPRAGE device in the sagittal plane. The imaging parameters were as follows: TR/TE = 1900/2.53 ms, TI = 900 ms, flip angle = 9°, FOV = 21.0 cm, section thickness = 1 mm, section gap = 0.5 mm, number of sections collected = 176, matrix = 192 × 192 × 256. An SWI sequence was performed to detect calcification and hemorrhagic areas. On the basis of advanced MR imaging, rCBF, FA, ADC, and MR spectra were calculated by the MR imaging console software program (syngo MR B17; Siemens).

Pulsed Arterial Spin-Labeling

We performed pulsed arterial spin-labeling perfusion MR imaging by using QUIPSS II with thin-slice TI1 periodic saturation (Q2TIPS).[22] The Q2TIPS technique is a pulsed arterial spin-labeling method that enables the acquisition of multiple sections. The inversion and saturation pulse parameters of Q2TIPS were set as follows: TI1 = 700 ms, TI1S = 1600 ms, and TI2 = 1800 ms. The other imaging parameters were as follows: TR/TE = 2800/13 ms, flip angle = 90°, FOV = 25.6 cm, section thickness = 8 mm, voxel size = 4 × 4 × 8 mm, section number = 9. Crusher gradients were not used. The total acquisition time was 4 minutes 19 seconds. Motion correction was interpolated according to the 3D *k*-space method, with a spatial filter setting of 2.0.

Diffusion Tensor Imaging

Axial DTI was performed by using single-shot spin-echo echo-planar imaging sequences. The parameters were as follows: TR/TE = 9200/96 ms, FOV = 23.0 cm, matrix = 128 × 128, b=0 s/mm^2 as reference imaging and b=1000 s/mm^2, diffusion-sensitive dimensions = 12, average = 3, scanning time = 6 minutes 28 seconds.

PASL and Diffusion Tensor Images

After reconstruction, the PASL, FA, and ADC images were converted into the DICOM format and inserted into the data base. To minimize confounding factors in the analysis, we kept the size of the ROIs in the lesion and contralateral normal brain constant (diameter = 8.0 mm) on both the PASL and diffusion tensor images. Two observers placed 5 ROIs each within the solid tumor component and 1 region of interest each in the contralateral normal brain.[6] Whenever possible, the ROIs were placed in mirrored white matter regions; when this placement was not possible, the ROIs were positioned in representative normal white matter in the same transaxial plane.[14] Care was taken to ensure that the ROIs were entirely within the solid part of the lesion to avoid contamination of the region of interest from normal tissue, areas of necrosis, cysts, hemorrhage, or intratumoral mineralization. We placed the ROIs at the site of the enhanced lesions on the contrast-enhanced T1-weighted MR images. In patients with nonenhancing tumors, the tumor parenchyma was identified as the area of hyperintensity on T2-weighted and FLAIR images. The ROIs were evaluated for eligibility independently by 2 authors (H.F. and T.S.), and any disagreements were resolved by consensus.

The rCBF, FA, and ADC ratios were calculated as follows: rCBF (FA or ADC) ratio = rCBF (FA or ADC) [tumor] / rCBF (FA or ADC) [contralateral normal tissue]. The average values of the minimum, maximum, and mean of the rCBF, FA, and ADC ratios were then selected for the analysis.

MR Spectroscopy

A single-voxel water-suppressed point-resolved spectroscopy sequence and multivoxel chemical shift imaging were performed. The single-voxel water-suppressed point-resolved spectroscopy sequence was performed by using the following parameters: TR/TE = 2000/270 ms, flip angle = 90°, voxel size = 20 × 20 × 20 mm (normal-sized lesion) or 15 × 15 × 15 mm (small lesion: lesions measuring less than approximately 20 mm in diameter), acquisition average = 192 (normal-sized lesion) or 256 (small lesion). The total acquisition time was 6 minutes 32 seconds (normal-sized lesion) or 8 minutes 40 seconds (small lesion). Multivoxel chemical shift imaging was performed by using the following parameters: TR/TE = 1700/270 ms, flip angle = 90°, FOV = 16.0 cm, section thickness = 8 mm, voxel size = 10 × 10 × 8 mm, acquisition average = 5. The total acquisition time was 9 minutes 26 seconds. The single-voxel water-suppressed point-resolved spectroscopy sequence was primarily performed; however, multivoxel chemical shift imaging was performed in cases of deep and centrally located tumors measuring >3 cm in diameter because for some temporal lobe and inferior frontal lobe tumors, adequate shimming can be problematic, while for intraventricular tumors and/or very peripheral tumors, CSF or scalp fat contamination may adversely affect MR spectroscopy acquisition. We selected the region of interest of the multivoxel area in the center region to prevent the influence of magnetic susceptibility and to optimize the shimming procedure. To the extent possible, we selected the multivoxel technique because the previous literature suggests that multivoxel MR spectroscopy is more useful for distinguishing glioma recurrence from posttreatment effects than single-voxel MR spectroscopy.[23]

The spectra were automatically analyzed for the relative signal intensity (area under the fitted peaks in the time domain) of the following metabolites: Cho, Cr, NAA, and Lac. The ratios of Cho/Cr, NAA/Cho, NAA/Cr, and Lac/Cr at TE 270 ms were calculated. The postprocessing steps, including the frequency shift, baseline correction, phase correction, and peak fitting/analysis, were performed first automatically and then manually. All spectral analyses were conducted within a window from 0.50 to 4.30 ppm (by using the standard method of assigning a shift value of 4.7 ppm to the measured unsuppressed water peak). The metabolite peak areas were assigned as follows: Cho, 3.20 ppm; Cr, 3.02 ppm; NAA, 2.00 ppm; Lac, 1.29 ppm. To avoid contamination of the voxel from normal tissue or areas of necrosis or cysts based on conventional MR imaging, we obtained the metabolite ratios within the solid portion of the lesion by consensus without knowledge of the final histologic tumor diagnosis.

Immunohistologic Assay

For Ki-67 immunostaining, the specimens were sliced from formalin-fixed, paraffin-embedded tissues. We stained the sections with a mouse anti-Ki-67 monoclonal antibody (MIB-1; Dako Cytomation, Carpinteria, California; 1:50 dilution). The Ki-67 labeling index, defined as the number of positive tumor cells / the total number of tumor cells × 100%, was calculated for at least 10 fields selected at random under a magnification ×400.

Statistical Analysis

We compared the MR imaging parameters and the Ki-67 labeling index in each of 3 groups (grade II versus grade III versus grade IV) by using the Tukey-Kramer test. The sensitivity, specificity, PPV, and NPV were calculated by using an ROC analysis to correctly identify high-grade gliomas (grade III and IV) and glioblastomas (grade IV), to differentiate the 2 groups, such as patients with high- and low-grade gliomas and those with glioblastomas and other-grade gliomas (grade II and III). Because oligodendroglial tumors tend to demonstrate hyperperfusion relative to astrocytic tumors, we also analyzed the CBF data only for purely astrocytic tumors that did not contain oligodendroglial regions, such as diffuse astrocytomas, anaplastic astrocytomas, and glioblastomas. The optimal threshold values were those that did the following: 1) minimized the observed number of instances of tumor-grade misclassification (C2 error = fraction of misclassified tumors), and 2) maximized the average observed sensitivity and specificity (C1 error) resulting in C1 = 1 − (sensitivity + specificity) / 2. To determine the combination of the most discriminative parameters, we used a stepwise multiple logistic backwards regression. The logistic regression was selected by using a cutoff level of .05 for significance. The correlations between the MR imaging parameters and the Ki-67 labeling index were analyzed statistically by using a Spearman correlation coefficient analysis.

RESULTS

Among 32 patients, 9 tumors were grade II (3 each of diffuse astrocytoma, oligodendroglioma, and oligoastrocytoma), 8 tumors grade III (3 anaplastic astrocytomas, 4 anaplastic oligodendrogliomas, and 1 anaplastic oligoastrocytoma), and 15 tumors grade IV (14 glioblastomas and 1 glioblastoma with an oligodendroglioma component). The patients included 13 men and 19 women, with a mean age of 59.8 ± 16.8 years. The conventional MR imaging characteristics of the tumors are shown in the Online Table. Patient 27 was unable to undergo an examination by using contrast agent due to her current treatment with dialysis. We performed multivoxel MR spectroscopy in 9 cases and single-voxel MR spectroscopy in 23 cases. Examples of low-grade and high-grade glial neoplasms are provided in Figs 1 and 2, respectively.

Both the mean ADC ratio ($r = -0.455$, $P = .0113$) and maximum ADC ratio ($r = -0.352$, $P = .0497$) exhibited a negative correlation with the Ki-67 index. In particular, there was a significant negative correlation between the minimum ADC ratio and the Ki-67 index ($r = -0.470$, $P = .0089$). A positive correlation was also observed between the Cho/Cr ratio and the Ki-67 index ($r = 0.461$, $P = .0103$) and between the Lac/Cr ratio and the Ki-67 index ($r = 0.418$, $P = .0199$). In contrast, no significant correlations were noted between the other parameters and the Ki-67 index.

The maximum rCBF ratio of the grade IV gliomas was higher than that of the grade III gliomas, while the Ki-67 labeling index of the grade II gliomas was lower than that of the grade III and grade IV gliomas ($P < .05$). The maximum FA ratio associated with grade II gliomas was lower than that associated with the grade IV gliomas, while the mean and minimum ADC ratios of grade II gliomas were higher than those of grade IV gliomas ($P < .05$).

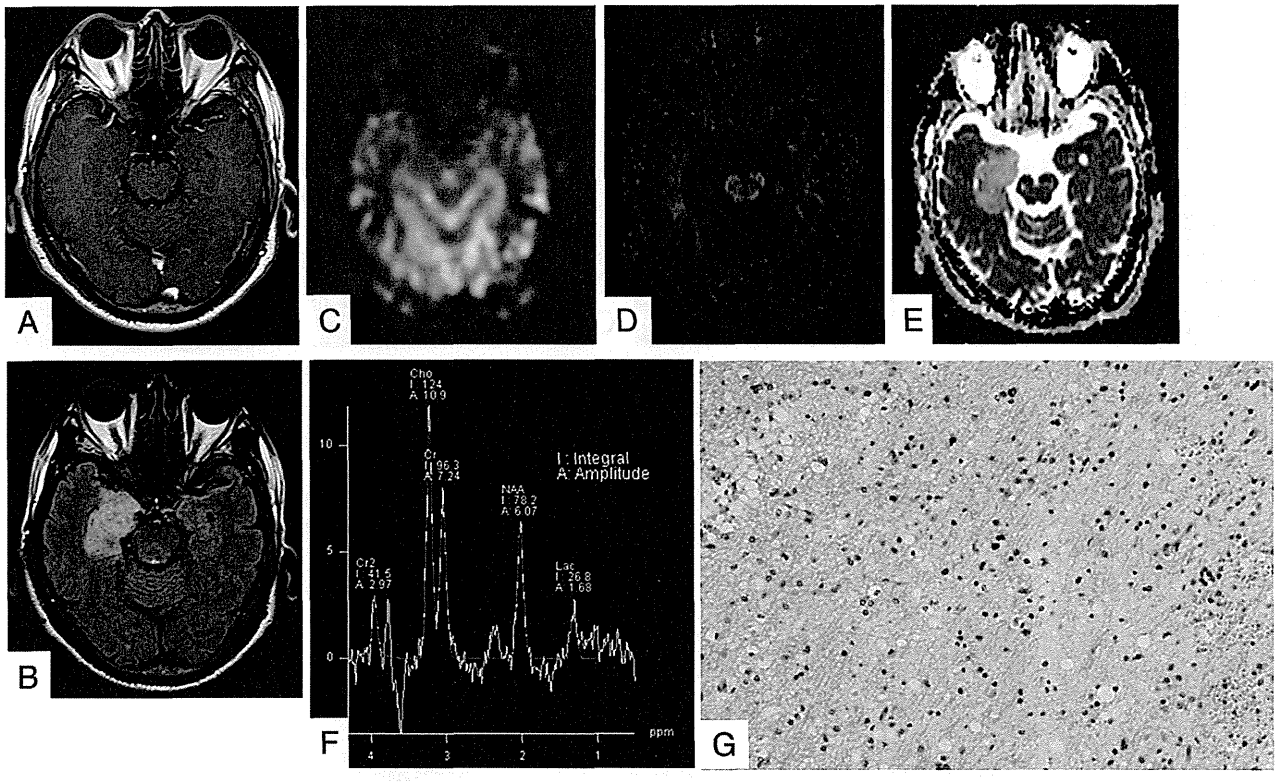

FIG 1. A 62-year-old man with a grade II oligoastrocytoma. The contrast-enhanced T1-weighted image shows a nonenhancing mass in the right hippocampus (*A*). The lesions presented high-intensity signals on FLAIR images (*B*). The rCBF map on PASL shows no areas of hyperperfusion (*C*). The FA map shows low FA values (*D*). The ADC map shows increased tumor diffusion values (*E*). The tumor MR spectrum shows decreased NAA and slightly increased Cho and Lac (*F*). The Ki-67 labeling index is 5.0% (original magnification × 400) (*G*).

Other comparisons did not reveal any statistically significant differences.

Regarding the parameters calculated from PASL, DTI, and MR spectroscopy, the threshold values were obtained separately for the minimum C1 and C2 errors, as shown in Tables 1 and 2. With respect to individual parameters for separating high-grade from low-grade gliomas, a threshold value of 1.789 for the Lac/Cr ratio, which exhibited the best performance for a minimum C1 error, provided sensitivity, specificity, PPV, and NPV of 73.9%, 100.0%, 100.0%, and 60.0%, respectively. Meanwhile, a threshold value of 1.789 for the Cho/Cr ratio, which exhibited the best performance for a minimum C2 error, provided sensitivity, specificity, PPV, and NPV of 91.3%, 77.8%, 91.3%, and 77.8%, respectively. Regarding individual parameters for separating glioblastomas from other-grade gliomas, a threshold value of 2.845 for the maximum rCBF ratio, which exhibited the best performance for minimum C1 and C2 errors, provided sensitivity, specificity, PPV, and NPV of 86.7%, 82.4%, 81.3%, and 87.5%, respectively. In particular, for evaluating purely astrocytic tumors, both the mean and maximum rCBF ratios demonstrated sensitivity, specificity, PPV, and NPV of 92.9%, 83.3%, 92.8%, and 83.4%, respectively.

According to multivariate logistic regression analysis, the combinations of parameters for differentiating high- and low-grade gliomas included the minimum ADC and Cho/Cr ratios, while those for differentiating glioblastomas and other-grade gliomas included the maximum rCBF and mean ADC ratios. The results of the ROC analyses by using these combinations are shown in Tables 3 and 4. The combination of the minimum ADC ratio and the Cho/Cr ratio provided sensitivity, specificity, PPV, and NPV of 87.0%, 88.9%, 95.2%, and 72.7%, respectively, for minimum C1 and C2 errors for differentiating high- and low-grade gliomas. Meanwhile, the combination of the maximum rCBF ratio and the mean ADC ratio provided sensitivity, specificity, PPV, and NPV of 73.3%, 94.1%, 91.7%, and 80.0%, respectively, for minimum C1 and C2 errors for differentiating glioblastomas and other-grade gliomas. This combination appears to be inferior compared with the minimum C1 and C2 errors of the maximum rCBF ratio; however, its accuracy was 84.4%, which is as high as that observed for the maximum rCBF ratio.

DISCUSSION

Cerebral gliomas are important and the most common primary brain tumors. MR imaging plays a critical role in the preoperative assessment and grading of gliomas. The classification and grading of gliomas on conventional MR imaging are sometimes unreliable. The sensitivity, specificity, PPV, and NPV for identifying high-grade gliomas on conventional MR imaging are 72.5%, 65.0%, 86.1%, and 44.1%, respectively.[15] The current study demonstrated contrast enhancement in 66.7%, 75.0%, and 100% of grade II, III, and IV gliomas, respectively, which suggests that it is difficult to perform glioma grading by only using structural gadolinium-enhanced MR imaging.[17] Physicians must perform a biopsy or surgical resection to make a pathologic diagnosis and evaluate the need for postoperative chemoradiotherapy. However, lesions for which the risks of biopsy are high cannot be accurately diagnosed and graded. The noninvasive evaluation of

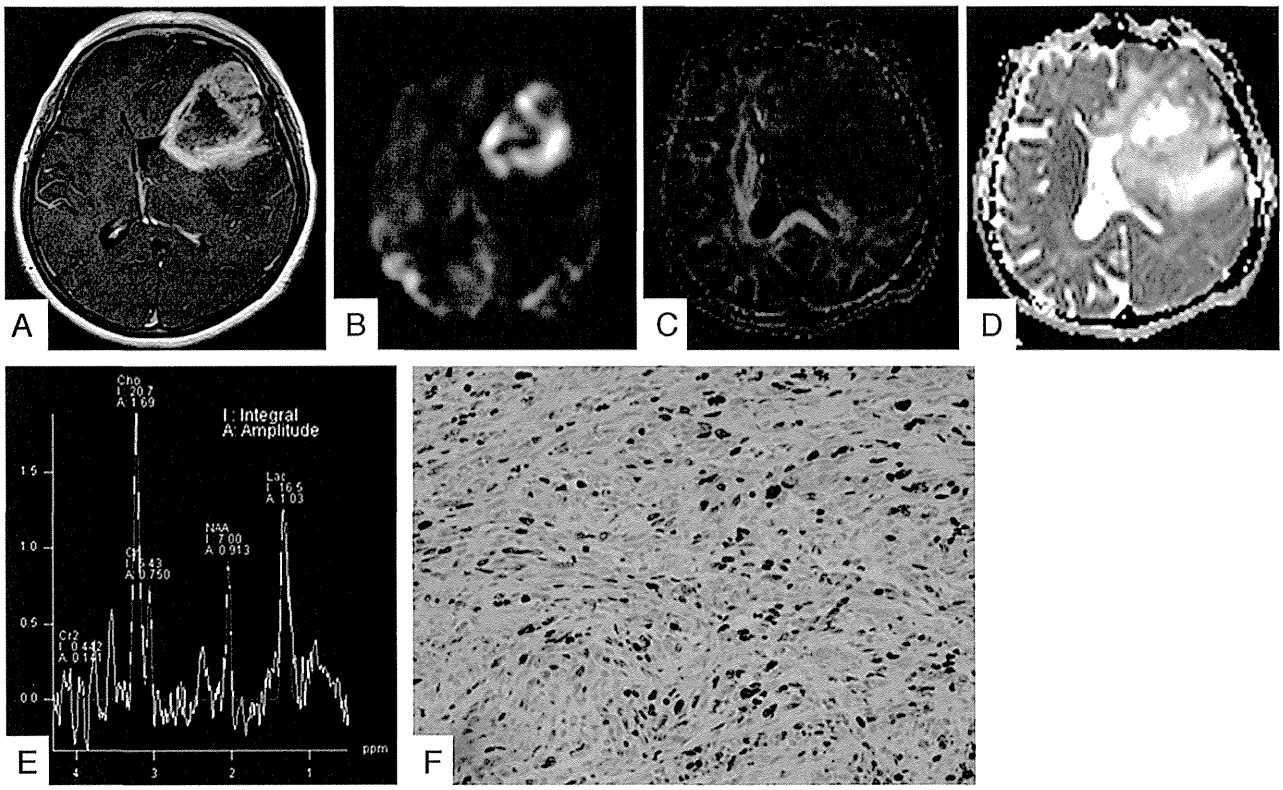

FIG 2. A 60-year-old woman with a grade IV glioblastoma. The lesion on the left frontotemporal lobe exhibits strong enhancement on gadolinium T1-weighted image (*A*). The neoplasm is clearly hyperperfused compared with the healthy parenchyma on the PASL image (*B*). The FA map shows slightly low FA values (*C*). The ADC map shows heterogeneous tumor diffusion values (*D*). The tumor MR spectrum shows decreased NAA with a marked increase in Cho and Lac (*E*). The Ki-67 labeling index is 27.0% (original magnification × 400) (*F*).

Table 1: Threshold values for multiple parameters for differentiating high- and low-grade gliomas

	Based on Minimum C1 Error					Errors		Based on Minimum C2 Error					Errors	
Parameters	Threshold	Sensitivity	Specificity	PPV	NPV	C1	C2	Threshold	Sensitivity	Specificity	PPV	NPV	C1	C2
rCBF ratio mean	2.562	0.652	0.778	0.882	0.467	0.285	0.170	2.562	0.652	0.778	0.882	0.467	0.285	0.170
rCBF ratio max	2.845	0.609	0.778	0.875	0.438	0.307	0.202	2.845	0.609	0.778	0.875	0.438	0.307	0.202
rCBF ratio min	2.017	0.739	0.667	0.850	0.500	0.297	0.179	2.017	0.739	0.667	0.850	0.500	0.297	0.179
rCBF ratio mean[a]	1.800	0.824	0.667	0.933	0.401	0.255	0.142	1.800	0.824	0.667	0.933	0.401	0.255	0.142
rCBF ratio max[a]	2.258	0.765	0.667	0.929	0.334	0.284	0.166	2.258	0.765	0.667	0.929	0.334	0.284	0.166
rCBF ratio min[a]	1.254	0.882	0.667	0.938	0.499	0.226	0.125	1.254	0.882	0.667	0.938	0.499	0.226	0.125
FA ratio mean	0.236	0.870	0.556	0.834	0.626	0.287	0.214	0.267	0.739	0.667	0.850	0.500	0.297	0.179
FA ratio max	0.288	0.870	0.667	0.870	0.668	0.232	0.128	0.288	0.870	0.667	0.870	0.668	0.232	0.128
FA ratio min	0.279	0.565	0.667	0.813	0.375	0.384	0.300	0.279	0.565	0.667	0.813	0.375	0.384	0.300
ADC ratio mean	1.659	0.913	0.667	0.875	0.750	0.210	0.118	1.659	0.913	0.667	0.875	0.750	0.210	0.118
ADC ratio max	1.538	0.826	0.556	0.826	0.556	0.309	0.227	1.538	0.826	0.556	0.826	0.556	0.309	0.227
ADC ratio min	1.564	0.913	0.667	0.875	0.750	0.210	0.118	1.564	0.913	0.667	0.875	0.750	0.210	0.118
Cho/Cr	1.789	0.913	0.778	0.913	0.778	0.155	0.057	1.789	0.913	0.778	0.913	0.778	0.155	0.057
NAA/Cho	0.349	0.696	0.778	0.889	0.500	0.263	0.142	0.349	0.696	0.778	0.889	0.500	0.263	0.142
NAA/Cr	1.289	0.304	1.000	1.000	0.360	0.348	0.484	0.894	0.478	0.778	0.846	0.368	0.372	0.322
Lac/Cr	1.789	0.739	1.000	1.000	0.600	0.131	0.068	1.789	0.739	1.000	1.000	0.600	0.131	0.068

Note:—min indicates minimum; max, maximum.

[a] rCBF ratios derived from purely astrocytomas.

gliomas results in a more precise assessment for selecting the surgical approach or chemoradiotherapy.

In the present study, the combination of the minimum ADC ratio and the Cho/Cr ratio exhibited a high sensitivity and specificity for distinguishing high- and low-grade gliomas. The mean ADC and minimal ADC values have been reported to be correlated with the tumor cell attenuation and thus used to grade astrocytomas.[10,14] In addition, the ADC ratio has been reported to be useful for grading gliomas.[18] Past studies have revealed that the Cho/Cr ratio tends to increase as glioma malignancy progresses.[13,18] Furthermore, Server et al[18] reported a minimum ADC ratio threshold value of 1.41 and a Cho/Cr threshold value of 1.35 for dividing high- and low-grade gliomas, similar to the results of our analysis. Published data regarding intracranial tumors indicate that a high ADC is attributable to a low level of cellularity, necrosis, or cysts, while a lower ADC is attributable to the presence of an attenuated, highly cellular tumor. The typical spectrum corresponding to a tumor shows an increased Cho peak, which corresponds to increased cell attenuation and membrane turnover in neoplastic tissue. With respect to glioma grading, our results consistently reflect the mitotic activity and presence of microvascular proliferation.

Table 2: Threshold values for multiple parameters for differentiating glioblastomas and other-grade gliomas

	Based on Minimum C1 Error					Errors		Based on Minimum C2 Error					Errors	
Parameters	Threshold	Sensitivity	Specificity	PPV	NPV	C1	C2	Threshold	Sensitivity	Specificity	PPV	NPV	C1	C2
rCBF ratio mean	2.562	0.867	0.765	0.765	0.867	0.184	0.073	2.562	0.867	0.765	0.765	0.867	0.184	0.073
rCBF ratio max	2.845	0.867	0.824	0.813	0.875	0.155	0.049	2.845	0.867	0.824	0.813	0.875	0.155	0.049
rCBF ratio min	2.017	0.867	0.588	0.650	0.834	0.273	0.187	2.164	0.800	0.647	0.667	0.786	0.277	0.165
rCBF ratio mean[a]	1.857	0.929	0.833	0.928	0.834	0.119	0.033	1.857	0.929	0.833	0.928	0.834	0.119	0.033
rCBF ratio max[a]	2.258	0.929	0.833	0.928	0.834	0.119	0.033	2.258	0.929	0.833	0.928	0.834	0.119	0.033
rCBF ratio min[a]	2.164	0.786	0.833	0.917	0.625	0.191	0.074	2.164	0.786	0.833	0.917	0.625	0.191	0.074
FA ratio mean	0.380	0.733	0.765	0.733	0.765	0.251	0.127	0.380	0.733	0.765	0.733	0.765	0.251	0.127
FA ratio max	0.371	0.800	0.588	0.631	0.769	0.306	0.210	0.418	0.667	0.706	0.667	0.706	0.314	0.197
FA ratio min	0.333	0.600	0.647	0.600	0.647	0.377	0.285	0.333	0.600	0.647	0.600	0.647	0.377	0.285
ADC ratio mean	1.305	0.800	0.765	0.750	0.813	0.218	0.095	1.305	0.800	0.765	0.750	0.813	0.218	0.095
ADC ratio max	1.494	0.933	0.529	0.636	0.899	0.269	0.226	1.494	0.933	0.529	0.636	0.899	0.269	0.226
ADC ratio min	1.449	0.933	0.647	0.700	0.916	0.210	0.129	1.148	0.733	0.824	0.786	0.778	0.222	0.102
Cho/Cr	1.789	0.933	0.471	0.609	0.888	0.298	0.284	2.813	0.733	0.647	0.647	0.733	0.310	0.196
NAA/Cho	0.338	0.733	0.647	0.647	0.733	0.310	0.196	0.338	0.733	0.647	0.647	0.733	0.310	0.196
NAA/Cr	1.922	0.200	1.000	1.000	0.586	0.400	0.640	0.725	0.600	0.412	0.474	0.539	0.494	0.506
Lac/Cr	2.778	0.667	0.882	0.833	0.750	0.226	0.125	2.778	0.667	0.882	0.833	0.750	0.226	0.125

[a] rCBF ratio derived from purely astrocytomas.

Table 3: Combination of the minimum ADC ratio and Cho/Cr for differentiating high- and low-grade gliomas

Based on Minimum C1 Error				Errors		Based on Minimum C2 Error				Errors	
Sensitivity	Specificity	PPV	NPV	C1	C2	Sensitivity	Specificity	PPV	NPV	C1	C2
0.870	0.889	0.952	0.727	0.121	0.029	0.870	0.889	0.952	0.727	0.121	0.029

Table 4: Combination of the maximum rCBF ratio and mean ADC ratio for differentiating glioblastomas and other-grade gliomas

Based on Minimum C1 Error				Errors		Based on Minimum C2 Error				Errors	
Sensitivity	Specificity	PPV	NPV	C1	C2	Sensitivity	Specificity	PPV	NPV	C1	C2
0.733	0.941	0.917	0.800	0.163	0.075	0.733	0.941	0.917	0.800	0.163	0.075

On the other hand, the maximum rCBF ratio, in addition to being helpful in combination with the mean ADC ratio, is most useful for differentiating glioblastomas and other-grade gliomas. The minimum ADC ratio was excluded in the logistic analysis, though the minimum ADC ratio of the glioblastomas was significantly lower than that of the other-grade lesions ($P < .05$). Perhaps, this is due to the inclusion of oligodendroglial tumors and astrocytic tumors in the assessment. It is surprising that the parameters obtained on MR spectroscopy did not demonstrate a high utility in differentiating glioblastomas from the remaining tumors. In particular, we did not expect that the sensitivity and specificity of the NAA/Cho ratio would be so low because prior studies have suggested that a prominent elevation of the Cho/NAA ratio is a hallmark of glioblastomas.[13,24] In the present study, we only evaluated astrocytomas, except for oligodendroglial tumors, and found that the maximum and mean rCBF ratios can be used to discriminate glioblastomas and other lesions, with C1 and C2 errors of 11.9% and 3.3%, respectively. Perfusion MR imaging is one of the most effective noninvasive methods for quantifying the grade of neoplastic neovascularization.[5,25-29] Furthermore, neovascularization is one of the most important criteria of malignancy for glioma grading. There has been extensive perfusion research related to predicting the glioma grade, much of it by using the DSC MR imaging technique.[27,28] On the other hand, ASL is a promising tool for assessing tumor angiogenesis and glioma grading.[2-7,26,29] ASL has several advantages, including being a nonionizing and completely noninvasive MR imaging technique that uses magnetically labeled arterial blood water protons as an endogenous tracer. For this reason, ASL is very suitable for diagnosing individuals with renal insufficiency and providing repeat follow-up.

Histologically, glioblastomas statistically have a larger microvessel attenuation than grade III lesions.[30] Previous studies have reported a positive correlation between rCBF-derived continuous ASL and vascular attenuation in gliomas.[3,5] Weber et al[16] attempted to elucidate the relationships between the rCBF on PASL and histopathologic findings, including the cell proliferation index and vessel attenuation, as defined by the number of microvessels. Our results indicated a high level of vascularity in glioblastomas and suggest that rCBF is a potential indicator of malignancy in gliomas based on vascular attenuation.

A multiparametric MR imaging approach has been attempted in past reports. Roy et al[17] studied 56 patients by using conventional MR imaging, DTI, dynamic contrast-enhanced perfusion imaging, and volumetric whole-brain MR spectroscopy and concluded that relative cerebral blood volume can be used to individually classify gliomas as low- or high-grade, with a sensitivity and specificity of 100% and 88%, respectively. On combining this parameter with the maximum relative cerebral blood volume, FA, ADC, and minimal NAA + Cr, classification was achieved with a 2% error and a sensitivity and specificity of 100% and 96%, respectively.[17] Unfortunately, the findings of the present study do not reach these levels of sensitivity and specificity; however, we used the ASL technique, which can measure the rCBF without a contrast agent. Weber et al[16] investigated the functional MR imaging methods DSC and PASL, dynamic contrast-enhanced MR imaging, and MR spectroscopy at 1.5T and suggested that the rCBF derived by using the PASL technique offers superior diagnostic performance in predicting the grade of gliomas. In another study of 1.5T, the combination of PASL and ADC significantly improved the sensitivity and predictive value of the preoperative

grading of gliomas compared with conventional imaging.[4] Only 1 study of the multiparametric MR imaging technique in combination with the ASL perfusion technique at 3T has been reported. Chawla et al[7] showed that the rCBF evaluated by using continuous ASL cannot be used to differentiate low-grade from high-grade gliomas, though the rCBF-guided voxel assessed by using a voxel analysis of multivoxel MR spectroscopy is useful for grading such tumors.

Histologically, we examined the Ki-67 labeling index as a marker of proliferation. Previous studies have shown that a higher rate of Ki-67-positive cells corresponds to greater malignancy and a worse survival rate in patients with gliomas.[19] Our studies demonstrated that the Ki-67 labeling index is correlated with MR imaging parameters, such as the ADC ratio, Cho/Cr ratio, and Lac/Cr ratio, consistent with the findings of previous literature.[20,21,31] These noninvasive imaging modalities can be used to reliably assess the potential for proliferation among brain tumors without a surgical procedure.

This study has several limitations. For example, the design included a relatively small population. In addition, when using diagnostic methods based on histologic biopsies, sampling bias should be considered. Although we used the same size region of interest for the multiple parameters of PASL, FA, and ADC, the region-of-interest diameter was relatively larger than that used in past reports and the effects of tumoral heterogeneity and regional differences were difficult to assess. Our method is based on the findings of an article by Hirai et al[6]; however, the placement of 5 ROIs on the ipsilesional side with only 1 region of interest on the contralateral side appears to be problematic for determining the ideal ratio. Regarding the limitation of the PASL sequence, a section thickness of 8 mm is relatively thick compared with that used in previous literature. We carefully placed the region of interest and minimized the potential for such errors. In the present study, we evaluated the data obtained by using both single-voxel and multivoxel techniques to secure the patients, though there may be a potential weaknesses in analyzing the combined single- and multivoxel MR spectroscopy data. Furthermore, the same TE conditions were used in each MR spectroscopy study to reduce the potential for error.

CONCLUSIONS

Our findings indicate that PASL, DTI, and MR spectroscopy provide useful parameters for predicting malignant grades of cerebral gliomas. In particular, the rCBF ratio calculated by using PASL at a high field strength is useful for distinguishing glioblastomas from grade II or III gliomas. The ADC, Cho/Cr, and Lac/Cr ratios have the potential to predict glioma proliferation.

REFERENCES

1. Louis DN, Ohgaki H, Wiestler OD, et al. **The 2007 WHO classification of tumours of the central nervous system.** *Acta Neuropathol* 2007;114:97–109
2. Warmuth C, Gunther M, Zimmer C. **Quantification of blood flow in brain tumors: comparison of arterial spin labeling and dynamic susceptibility weighted contrast-enhanced MR imaging.** *Radiology* 2003;228:523–32
3. Kimura H, Takeuchi H, Koshimoto Y, et al. **Perfusion imaging of meningioma by using continuous arterial spin-labeling: comparison with dynamic susceptibility-weighted contrast-enhanced MR images and histopathologic features.** *AJNR Am J Neuroradiol* 2006;27:85–93
4. Kim HS, Kim SY. **A prospective study on the added value of pulsed arterial spin-labeling and apparent diffusion coefficients in the grading of gliomas.** *AJNR Am J Neuroradiol* 2007;28:1693–99
5. Noguchi T, Yoshiura T, Hiwatashi A, et al. **Perfusion imaging of brain tumors using arterial spin-labeling: correlation with histopathologic vascular density.** *AJNR Am J Neuroradiol* 2008;29:688–93
6. Hirai T, Kitajima M, Nakamura H, et al. **Quantitative blood flow measurements in gliomas using arterial spin-labeling at 3T: intermodality agreement and inter- and intraobserver reproducibility study.** *AJNR Am J Neuroradiol* 2011;32:2073–79
7. Chawla S, Wang S, Wolf RL, et al. **Arterial spin-labeling and MR spectroscopy in the differentiation of gliomas.** *AJNR Am J Neuroradiol* 2007;28:1683–89
8. Zikou AK, Alexiou GA, Kosta P, et al. **Diffusion tensor and dynamic susceptibility contrast MRI in glioblastoma.** *Clin Neurol Neurosurg* 2012;114:607–12
9. Liu X, Tian W, Kolar B, et al. **MR diffusion tensor and perfusion-weighted imaging in preoperative grading of supratentorial nonenhancing gliomas.** *Neuro Oncol* 2011;13:447–55
10. Lee EJ, Lee SK, Agid R, et al. **Preoperative grading of presumptive low-grade astrocytomas on MR imaging: diagnostic value of minimum apparent diffusion coefficient.** *AJNR Am J Neuroradiol* 2008;29:1872–77
11. Yang D, Korogi Y, Sugahara T, et. al. **Cerebral gliomas: prospective comparison of multivoxel 2D chemical-shift imaging proton MR spectroscopy, echoplanar perfusion and diffusion-weighted MRI.** *Neuroradiology* 2002;44:656–66
12. Zou QG, Xu HB, Liu F, et al. **In the assessment of supratentorial glioma grade: the combined role of multivoxel proton MR spectroscopy and diffusion tensor imaging.** *Clin Radiol* 2011;66:953–60
13. Li X, Lu Y, Pirzkall A, et al. **Analysis of the spatial characteristics of metabolic abnormalities in newly diagnosed glioma patients.** *J Magn Reson Imaging* 2002;16:229–37
14. Di Costanzo A, Scarabino T, Trojsi F, et al. **Multiparametric 3T MR approach to the assessment of cerebral gliomas: tumor extent and malignancy.** *Neuroradiology* 2006;48:622–31
15. Law M, Yang S, Wang H, et al. **Glioma grading: sensitivity, specificity, and predictive values of perfusion MR imaging and proton MR spectroscopic imaging compared with conventional MR imaging.** *AJNR Am J Neuroradiol* 2003;24:1989–98
16. Weber MA, Zoubaa S, Schlieter M, et al. **Diagnostic performance of spectroscopic and perfusion MRI for distinction of brain tumors.** *Neurology* 2006;66:1899–906
17. Roy B, Gupta RK, Maudsley AA, et al. **Utility of multiparametric 3-T MRI for glioma characterization.** *Neuroradiology* 2013;55:603–13
18. Server A, Kulle B, Gadmar ØB, et al. **Measurements of diagnostic examination performance using quantitative apparent diffusion coefficient and proton MR spectroscopic imaging in the preoperative evaluation of tumor grade in cerebral gliomas.** *Eur J Radiol* 2011:80:462–70
19. Johannessen AL, Torp SH. **The clinical value of Ki-67/MIB-1 labeling index in human astrocytomas.** *Pathol Oncol Res* 2006;12:143–47
20. Guillevin R, Menuel C, Duffau H, et al. **Proton magnetic resonance spectroscopy predicts proliferative activity in diffuse low-grade gliomas.** *J Neurooncol* 2008;87:181–87
21. Yin Y, Tong D, Liu X, et al. **Correlation of apparent diffusion coefficient with Ki-67 in the diagnosis of gliomas.** *Zhongguo Yi Xue Ke Xue Yuan Xue Bao* 2012:34:503–08
22. Luh WM, Wong EC, Bandettini PA, et al. **QUIPSS II with thin-slice TI1 periodic saturation: a method for improving accuracy of quantitative perfusion imaging using pulsed arterial spin labeling.** *Magn Reson Med* 1999;41:1246–54
23. Fink JR, Carr RB, Matsusue E, et al. **Comparison of 3 Tesla proton MR spectroscopy, MR perfusion and MR diffusion for distinguish-**

ing glioma recurrence from posttreatment effects. *J Magn Reson Imaging* 2012;35:56–63
24. Magalhaes A, Godfrey W, Shen Y, et al. **Proton magnetic resonance spectroscopy of brain tumors correlated with pathology.** *Acad Radiol* 2005;12:51–57
25. Cha S, Knopp EA, Johnson G, et al. **Intracranial mass lesions: dynamic contrast-enhanced susceptibility-weighted echo-planar perfusion MR imaging.** *Radiology* 2002;223:11–29
26. Järnum H, Steffensen EG, Knutsson L, et al. **Perfusion MRI of brain tumours: a comparative study of pseudo-continuous arterial spin labelling and dynamic susceptibility contrast imaging.** *Neuroradiology* 2010;52:307–17
27. Aronen HJ, Gazit IE, Louis DN, et al. **Cerebral blood volume maps of gliomas: comparison with tumor grade and histologic findings.** *Radiology* 1994;191:41–51
28. Knopp EA, Cha S, Johnson G, et al. **Glial neoplasms: dynamic contrast-enhanced T2*-weighted MR imaging.** *Radiology* 1999;211:791–98
29. Kim MJ, Kim HS, Kim JH, et al. **Diagnostic accuracy and interobserver variability of pulsed arterial spin labeling for glioma grading.** *Acta Radiol* 2008;49:450–57
30. Sharma S, Sharma MC, Gupta DK, et al. **Angiogenic patterns and their quantitation in high grade astrocytic tumors.** *J Neurooncol* 2006;79:19–30
31. Calvar JA, Meli FJ, Romero C, et al. **Characterization of brain tumors by MRS, DWI and Ki-67 labeling index.** *J Neurooncol* 2005;72:273–80

Neuro-Oncology Advance Access published November 26, 2013

Neuro-Oncology

Neuro-Oncology 2013; **0**, 1–7, doi:10.1093/neuonc/not144

H3F3A K27M mutations in thalamic gliomas from young adult patients

Koki Aihara, Akitake Mukasa, Kengo Gotoh, Kuniaki Saito, Genta Nagae, Shingo Tsuji, Kenji Tatuno, Shogo Yamamoto, Shunsaku Takayanagi*, Yoshitaka Narita, Soichiro Shibui, Hiroyuki Aburatani and Nobuhito Saito

Department of Neurosurgery, Graduate School and Faculty of Medicine, The University of Tokyo, Tokyo, Japan (K.A., A.M., K.S., S.T., N.S.); Genome Science Division, Research Center for Advanced Science and Technology, The University of Tokyo, Tokyo, Japan (K.A., K.G., G.N., S.T., K.T., S.Y., H.A.); Department of Neurosurgery and Neuro-Oncology, National Cancer Center Hospital, Tokyo, Japan (Y.N., S.S.)*

Corresponding authors: Akitake Mukasa, MD, PhD, Department of Neurosurgery, The University of Tokyo Hospital, 7-3-1 Hongo, Bunkyo-ku, Tokyo 113-8655, Japan (mukasa-nsu@umin.ac.jp); Hiroyuki Aburatani, MD, PhD, Genome Science Division, Research Center for Advanced Science and Technology (RCAST), The University of Tokyo, 4-6-1 Komaba, Meguro-ku, Tokyo 153-8904, Japan (haburata-tky@umin.ac.jp).

Introduction: Mutations in *H3F3A*, which encodes histone H3.3, commonly occur in pediatric glioblastoma. Additionally, *H3F3A* K27M substitutions occur in gliomas that arise at midline locations (eg, pons, thalamus, spine); moreover, this substitution occurs mainly in tumors in children and adolescents. Here, we sought to determine the association between *H3F3A* mutations and adult thalamic glioma.

Methods: Genomic *H3F3A* was sequenced from 20 separate thalamic gliomas. Additionally, for 14 of the 20 gliomas, 639 genes—including cancer-related genes and chromatin-modifier genes—were sequenced, and the Infinium HumanMethylation450K BeadChip was used to examine DNA methylation across the genome.

Results: Of the 20 tumors, 18 were high-grade thalamic gliomas, and of these 18, 11 were from patients under 50 years of age (median age, 38 y; range, 17–46), and 7 were from patients over 50 years of age. The *H3F3A* K27M mutation was present in 10 of the 11 (91%) younger patients and absent from all 7 older patients. Additionally, *H3F3A* K27M was not detected in the 2 diffuse astrocytomas. Further sequencing revealed recurrent mutations in *TP53*, *ATRX*, *NF1*, and *EGFR*. Gliomas with *H3F3A* K27M from pediatric or young adult patients had similar, characteristic DNA methylation profiles. In contrast, thalamic gliomas with wild-type *H3F3A* had DNA methylation profiles similar to those of hemispheric glioblastomas.

Conclusion: We found that high-grade thalamic gliomas from young adults, like those from children and adolescents, frequently had *H3F3A* K27M.

Keywords: thalamic glioma, young adult, *H3F3A* mutation.

Gliomas of the thalamic region are relatively rare and constitute ~1% of all brain tumors.[1–3] Thalamic gliomas are generally difficult to treat because the tumors are located deep within the brain and, therefore, are rarely amenable to radical surgical resection.[4] Thus, development of a novel anticancer drug is needed to treat these tumors. Schwartzentruber et al[5] recently reported that more than 30% of pediatric glioblastoma multiforme (GBM) tumors carry a mutation in the *H3F3A* gene, which encodes the replication-independent histone 3 variant H3.3. There are 2 common mutations (K27M and G34R/V) in human *H3F3A* that each result in an amino acid substitution within the histone tail. In a study of 784 glioma samples of all grades and histological diagnoses and from patients of all ages, the *H3F3A* K27M mutation was highly specific to GBM and was found mainly in younger patients (median age, 11 y; range, 5–29), including several patients with thalamic GBM. Wu et al[6] also reported a high frequency of *H3F3A* mutations in pediatric gliomas and that 78% of diffuse intrinsic pontine gliomas (DIPGs) and 22% of nonbrainstem pediatric GBM carry a mutation in *H3F3A* or in a related gene, *HIST1H3B*, which encodes the histone H3.1; each of these mutations causes a K27M amino acid substitution in the respective protein. Sturm et al[7] further showed that these mutant tumors have distinct methylation profiles and that the *H3F3A* K27M mutation most often occurs in tumors located in the midline of the brain, such as in the thalamus, brainstem, or spine. In contrast, G34R/V mutations were found in hemispheric gliomas. Although 71%–78% of DIPGs are known to have a K27M mutation,[6,8] to our knowledge no study has focused on the *H3F3A* K27M mutation in thalamic gliomas. Here, we analyzed the prevalence and significance of the K27M mutation, especially for adult patients with thalamic glioma.

Received 16 May 2013; accepted 4 August 2013

Materials and Methods

Patients and Samples

From April 1997 to March 2013, 27 adult patients (>16 y of age) with primary thalamic glioma were treated at Tokyo University Hospital or the National Cancer Center Hospital (Table 1). Histological diagnoses were made by a senior neuropathologist from the respective treatment centers and according to World Health Organization guidelines. There were 15 GBM, 9 anaplastic astrocytomas (AAs), and 3 diffuse astrocytomas (DAs). Of the 3 low-grade gliomas, 2 were located bilaterally; in contrast, most high-grade gliomas were not bilateral (left, 12; right, 11; bilateral, 1). We were able to obtain samples of freshly frozen tumor tissue for 16 of the 27 cases; and for 14 of these 16 cases, paired, normal blood samples were available; moreover, formalin-fixed, paraffin-embedded samples of tumor tissue were available for 4 of the other 11 cases. In all, tissue samples were available for 20 of the 27 cases. The study was approved by the ethics committees of the University of Tokyo Hospital and the National Cancer Center Hospital. Each patient provided written informed consent.

DNA Extraction

The AllPrep DNA/RNA Micro kit (Qiagen) was used according to the manufacturer's instructions to extract genomic DNA from freshly frozen tumor tissue. Formalin-fixed, paraffin-embedded samples were deparaffinized with xylene, and a QIAamp DNA Mini kit (Qiagen) was then used to extract genomic DNA from these tumor samples. For the 14 cases for which tumor tissues and a paired, normal blood sample were available, a DNA extraction kit (Qiagen) was used to extract control genomic DNA from the paired blood sample.

Sanger Sequencing

For the 20 cases in which DNA from tumor tissue was available, the Sanger method was used to sequence the DNA. Oligo primers were designed to amplify a target region within *H3F3A* (sense 5′- TCAATGCTGGTAGGTAAG TAAGGA -3′, antisense 5′- GGTTTCTTCACCCCTCCAGT -3′; product size: 152 bp). The high-fidelity DNA polymerase KOD-plus (Toyobo) and optimized thermal conditions were used to perform PCR, and the PCR products

Table 1. Patient characteristics and *H3F3A* status

Sample ID	Age	Location	OS (mo)	Surgery	Treatment	*H3F3A*	*MGMT* Promoter
GBM1[a,b]	17	Right	8.9	PR	RT + TMZ	K27M	u
AA1	19	Bilateral	30.6	Biopsy	RT + ACNU	-	-
AA2[a,b]	20	Left	9.9	Biopsy	RT + TMZ	K27M	u
GBM2[a,b]	27	Multiple[d]	3.8	PR	RT + TMZ	K27M	u
GBM3[a,b]	34	Right	12.6	STR	RT + ACNU	K27M	u
AA3	37	Right	26.1	Biopsy	RT + TMZ	K27M	-
GBM4[a,b]	38	Left	9.8	Biopsy	RT + TMZ	K27M	u
AA4	38	Left	17.7	Biopsy	RT + ACNU	WT	-
GBM5[a,b]	39	Right	10.4	PR	RT + TMZ	K27M	u
AA5[b]	41	Left	20.6	PR	RT + TMZ	K27M	u
AA6[a,b]	43	Left	15.6	Biopsy	RT + TMZ	K27M	m
GBM6	45	Left	30.8	Biopsy	RT + ACNU	-	-
GBM7[a,b]	46	Right	1.6[f]	GTR	RT + TMZ	K27M	u
AA7	47	Right	24.3	Biopsy	RT + ACNU	-	-
GBM8	48	Left	65.8	Biopsy	RT + TMZ	-	-
GBM9[b]	50	Right	3.9	Biopsy	RT + TMZ	WT	u
GBM10	53	Left	7.3	Biopsy	RT + TMZ	-	-
AA8[a,b,c]	57	Multiple[e]	110.2[f]	Biopsy	RT + ACNU	WT	m
GBM11[a,b,c]	62	Left	19.4	Biopsy	RT + TMZ	WT	u
GBM12[a,b]	64	Left	30.4	STR	RT + TMZ	WT	m
GBM13[a]	71	Left	3.5	Biopsy	RT + TMZ	WT	-
GBM14	73	Left	17.9	Biopsy	RT + TMZ	-	-
GBM15[a,b]	73	Right	0.7	Biopsy	RT + TMZ	WT	u
AA9	78	Right	0.3	Biopsy	No therapy	WT	-
DA1	28	Bilateral	21.1	Biopsy		-	-
DA2[a]	29	Bilateral	9.2[f]	Biopsy		WT	-
DA3	30	Left	124.4[f]	Biopsy		WT	-

Abbreviations: OS, overall survival; GTR, gross total resection; STR, subtotal resection; PR, partial resection; RT, radiotherapy; TMZ, temozolomide; ACNU, nimustine hydrochloride; WT, wild-type; m, methylated; u, unmethylated; -, not available.
[a]Specimen subjected to targeted sequence analysis.
[b]Specimen subjected to global methylation profile analysis.
[c]Specimen of recurrence.
[d]Right thalamus, left temporal lobe, and fourth ventricle.
[e]Right thalamus, left cerebellopontine angle, cerebellum surface, and fourth ventricle.
[f]Still alive at last follow-up.

were then evaluated on a 2% agarose gel and subsequently purified. The Big Dye Terminator kit (Applied Biosystems) was used for each sequencing reaction; both strands of each PCR product were sequenced, and each sample was analyzed on an ABI 3130xl capillary sequencer (Applied Biosystems).

Targeted Sequencing

For the 14 cases for which a tumor sample and a paired, normal blood sample were available, we used the Haloplex system (Agilent) to amplify and analyze the sequences of 639 selected genes (see Supplementary Table S1). These selected genes included *H3F3A, HIST1H3B*, genes often mutated in gliomas (such as *IDH1/2, ATRX, TP53, NF1, EGFR, PDGFRA*), other frequently mutated cancer genes, and chromatin-modifier genes. Target regions were enriched using Haloplex technology following the manufacturer's protocols. A Hiseq2500 system (Illumina) set in rapid mode was used to sequence the amplified targets as 150-bp paired-end reads. The median coverage was 348-fold, and more than 93% of target regions were covered by at least 10 reads (see Supplementary Table S2). The Burrows-Wheeler Aligner algorithm v0.5.9[9] was used to map this sequence data onto the reference genome (hg19), and somatic mutations were identified with the Genome Analysis Toolkit Unified Genotyper v1.6.13.[10] The tumor-specific mutations were identified by comparing results from tumor DNA and blood DNA and were annotated with Annovar (23 October 2012).[11] Finally, we used the Integrative Genomics Viewer v2.2[12] to check these mutations, and we excluded artifact mutations.

Methylation-specific PCR

The EZ DNA Methylation kit (Zymo Research) was used according to the manufacturer's protocol to conduct bisulfite reactions with each genomic DNA sample (250 ng). DNA methylation status of the O^6-methylguanine methyltransferase (*MGMT*) promoter was then determined by methylation-specific PCR as described by Esteller et al.[13]

Global Analysis of DNA Methylation

The Infinium HumanMethylation450 BeadChip (Illumina) was used according to the manufacturer's instructions to examine the genome-wide DNA methylation profiles of 14 high-grade thalamic gliomas. Previously published[7] methylation data from additional glioblastoma samples ($n = 136$) and from control samples ($n = 6$; 2 adult normal brain and 4 fetal normal brain) were obtained from the National Center for Biotechnology Information's Gene Expression Omnibus (http://www.ncbi.nlm.nih.gov/geo). The following filtering steps were used to select probes for unsupervised clustering analysis. Probes targeting the X and Y chromosomes and probes containing a single nucleotide polymorphism (dbSNP130 common) within 5 base pairs of and including the targeted cytosine-phosphate-guanine (CpG) site were removed. The standard deviation of β-values for each probe was calculated, and the top 8000 probes were selected.

Statistical Analysis

Overall survival was analyzed using the Cox regression analysis or the Kaplan-Meier method, and the log-rank test was used to make universal assessments of Kaplan-Meier plots. The frequency of methylation of the *MGMT* promoter and of other genes was analyzed by Fisher's exact test, and Welch's *t*-test was used to compare the average age of the *H3F3A* K27M group with that of the wild-type *H3F3A* group. $P < .05$ was considered significant. Statistical calculations were carried out using R v2.15.2 (http://www.cran.r-project.org).

Results

Frequency and Characteristics of Patients Harboring the H3F3A *K27M Mutation*

Among the 18 high-grade thalamic gliomas that we subjected to sequence analysis, 10 (56%) tumors had an *H3F3A* K27M mutation, while none of the 18 tumors harbored an *H3F3A* mutation at G34. Remarkably, 10 (91%) of the 11 tumors that were from patients under 50 years of age (median age, 38 y; range, 17–46) had the *H3F3A* K27M mutation; in contrast, the *H3F3A* K27M mutation was not found in any of the 7 tumors that were from patients over 50 years of age (Table 1). The patients with the *H3F3A* K27M mutation were significantly younger than those with wild-type *H3F3A* alleles (34.2 vs 61.6 y; $P = .0003$). The *H3F3A* K27M mutation was not detected in DAs from patients who were 29 or 30 years of age.

Targeted Sequence Analyses for Selected Genes

Among the 14 cases that were subject to targeted sequence analysis, tumor DNA samples from cases GBM4 and GBM11 each had mutations in mismatch repair genes and had a higher than average number of mutations; the average number of nonsynonymous mutations in DNA samples from all tumors except these 2 GBM specimens was 3.83 (0–8) (see Supplementary Table S3), while the numbers of nonsynonymous mutations in the DNA samples from GBM4 and GBM11 were 32 and 165, respectively. GBM4 had a mutation in the mismatch repair gene *MSH2* (MutS homolog 2). In the case of GBM11, which recurred after treatment with the alkylating agent temozolomide, mutations were identified in 2 mismatch repair genes, *PMS2* (postmeiotic segregation increased 2) and *MLH3* (MutL homolog 3); moreover, 158 (96%) of 165 mutations found in this tumor were G/C to A/T transitions. Therefore, GBM11 apparently had a hypermutator phenotype.[14] Because most of the mutations in these 2 cases (GBM4 and GBM11) could have accumulated passively owing to the lack of mismatch repair function, we excluded the mutation data from these cases from the subsequent analyses.

Consistent with previously reported data,[5] *H3F3A*-mutant high-grade gliomas frequently also had mutations in *TP53, ATRX* (2/7 [28.6%] of *H3F3A* K27M-mutant tumors vs 0/4 [0%] of wild-type *H3F3A* tumors; $P = .49$), and *NF1* (3/7 [42.9%] vs 0/4 [0%]; $P = .24$) (Fig. 1). In contrast, wild-type *H3F3A* tumors had *EGFR* mutations more frequently than did *H3F3A* K27M-mutant tumors (0/7 [0%] vs 2/4 [50%]; $P = .11$). There were no recurrent mutations other than *H3F3A, TP53, ATRX, NF1*, and *EGFR*. Wu et al[6] reported that 18% of DIPGs had a *HIST1H3B* K27M mutation, but we did not find *HIST1H3B* mutations in any of the 14 tissue samples evaluated, even in samples from wild-type *H3F3A* tumors. Additionally, none of the 14 tumors examined had an *IDH1* or an *IDH2* mutation.

Recently, Fontebasso et al[15] found that mutations in the *SETD2* gene, which encodes an H3K36 trimethyltransferase, occurred in 15% of hemispheric pediatric GBMs, and mutations in *SETD2* and *H3F3A* were mutually exclusive. Based on these findings, we also sequenced genes that potentially affect histone modification, such as the H3K27 methyltransferase *EZH2*, the H3K27 demethylase *KDM6A*, the H3K27 acetyltransferase *EP300*, and *CREBBP*. We identified a *KDM6A* mutation (p.R1213L), located in

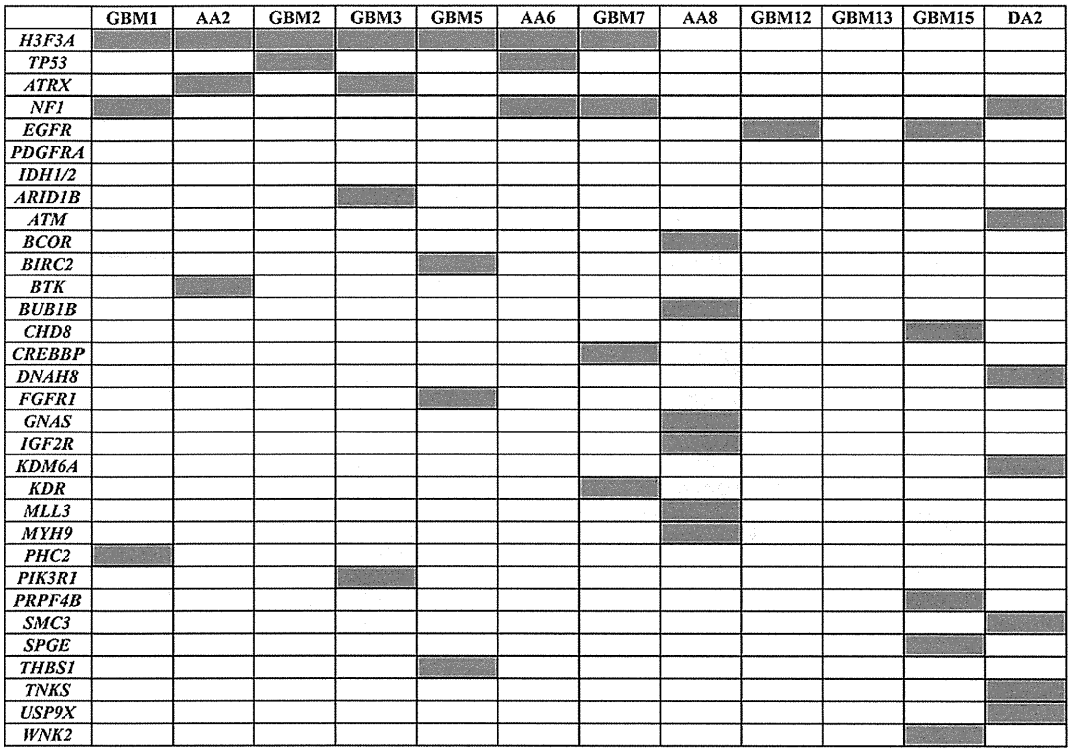

Fig. 1. Nonsynonymous mutations identified via targeted sequencing. Each row represents a specific gene, and each column represents one sample. The shaded boxes represent identified nonsynonymous mutations.

the JmjC domain, in one case of DA with wild-type *H3F3A* and a *CREBBP* mutation in one case of GBM with the *H3F3A* K27M mutation. However, we did not find mutations in any of these genes in any of the 4 analyzed cases of high-grade glioma that lacked an *H3F3A* K27M mutation.

In addition, we found an *FGFR1* mutation (N546K) in one GBM (GBM5) with *H3F3A* K27M. Schwartzentruber et al[5] also reported an *FGFR1* mutation (K656E) in an *H3F3A* K27M-mutant tumor.[3] Both of these *FGFR1* mutations reportedly enhance kinase activity.[15]

Methylation Status of the MGMT *Promoter*

We analyzed methylation at the *MGMT* promoter in samples from 14 adults with high-grade gliomas whose DNA was suitable for such analysis; the *MGMT* promoter in 11 (79%) of these tumors was unmethylated. In particular, the *MGMT* promoter was frequently unmethylated in samples of thalamic glioma with an *H3F3A* K27M mutation from young adults (8/9; 89%). The rate of unmethylated *MGMT* promoter was higher in the group of samples analyzed in this study than in a group of high-grade gliomas from all locations that we analyzed previously (43/75; 57%),[16] but the difference between these rates was not statistically significant ($P = .23$).

Global DNA Methylation Profiles of Thalamic Gliomas

The genome-wide Infinium methylation data demonstrated that adult thalamic high-grade gliomas with the *H3F3A* K27M mutation had methylation profiles distinct from those of adult thalamic high-grade gliomas that lacked the *H3F3A* K27M mutation (Fig. 2). In the hierarchal clustering analysis that included methylation profile data from previously categorized pediatric and adult gliomas,[7] the adult thalamic high-grade gliomas harboring the *H3F3A* K27M mutation clustered within the same "K27" category as did the pediatric gliomas harboring *H3F3A* K27M. In contrast, adult thalamic high-grade gliomas with wild-type *H3F3A*, which had a variety of methylation profiles, did not cluster into the K27 category, but clustered within several other categories, including "mesenchymal" and "classic." One recurrent anaplastic astrocytoma (AA8) that was wild-type for *H3F3A* had a profile that was similar to those of the tumors in the K27 category, but this profile seemed to be located outside the cluster in the K27 category.

Prognostic Value of the H3F3A *K27M Mutation*

For the 16 cases for which a primary tumor sample was analyzed, the median overall survival of patients with GBM and those with AA was 8.9 months and 15.6 months, respectively. The median overall survival of patients with high-grade gliomas (GBM or AA) was 9.9 months, and progression-free survival of these patients was 5.3 months. In these cases of high-grade glioma, the median overall survival of patients with *H3F3A* K27M-mutant tumors was 10.4 months (GBM, 9.8 mo; AA, 15.6 mo) and that of patients with wild-type *H3F3A* tumors was 3.5 months (GBM, 3.5 mo; AA, 0.3 mo). There was no statistical difference in overall survival ($P = .80$) or progression-free survival (6.0 vs 1.8; $P = .44$) between these 2 groups (Fig. 3).

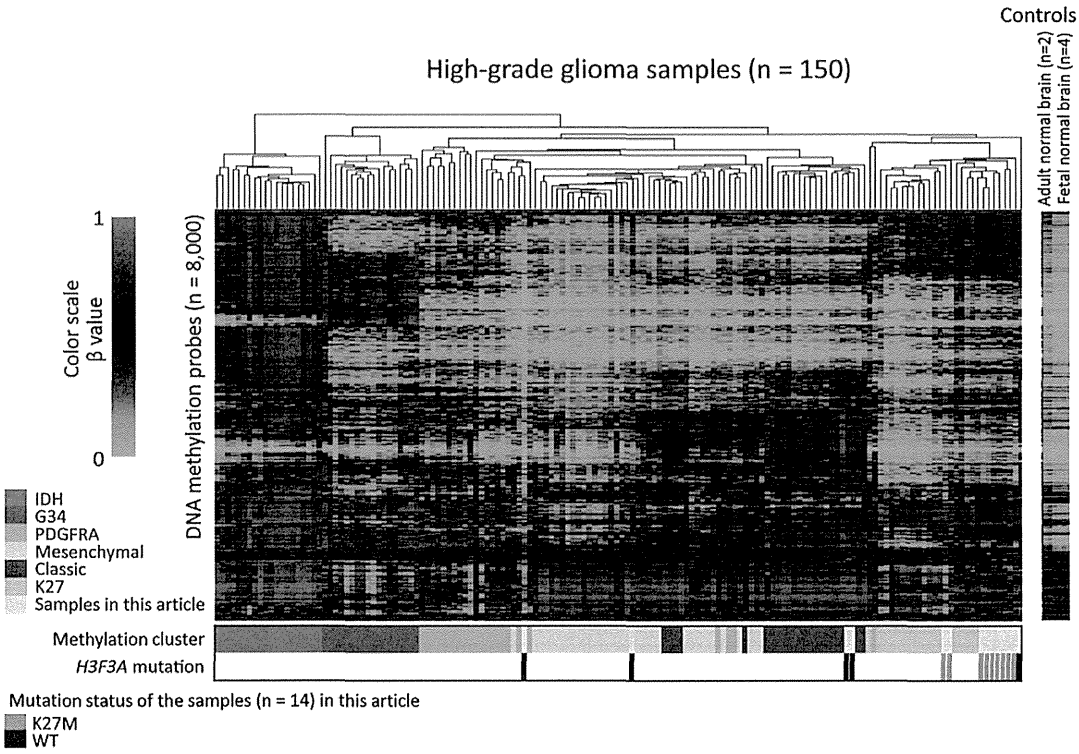

Fig. 2. Heatmap of methylation levels (β-value) in 150 high-grade gliomas, including 14 thalamic gliomas analyzed in this study. Supervised clustering was performed using 8000 selected Infinium probes. Each row represents a probe, each column represents one sample. For each sample, annotation of methylation cluster and *H3F3A* mutation status are indicated by colored boxes at the bottom of the map.

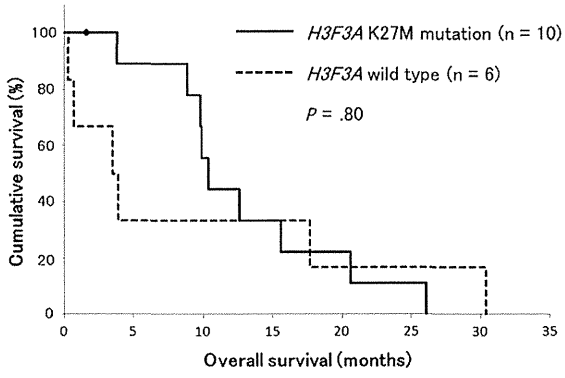

Fig. 3. Kaplan–Meier estimates of overall survival in cases of high-grade thalamic gliomas. There was no statistical difference in overall survival between patients with *H3F3A* K27M-mutant tumors and those with wild-type *H3F3A* tumors.

The Cox regression analysis assessing 3 variables—*H3F3A* K27M mutation status, *MGMT* methylation, and age—showed no significant difference in overall survival due to any one variable (*H3F3A* mutation: hazard ratio [HR] = 0.11, 95% confidence interval [CI] = 0.0057–2.2, $P = .15$; *MGMT* methylation: HR = 0.088, 95% CI = 0.0054–1.4, $P = .088$; and age: HR = 0.96, 95% CI = 0.88–1.1, $P = .38$).

Discussion

Here, we showed that the *H3F3A* K27M mutation was common in high-grade thalamic gliomas in young adults, as is the case for GBM in children and adolescents.[17] Reportedly, 80% of pediatric thalamic GBM tumors harbor the *H3F3A* K27M substitution,[5,7,17] as do 71%–78% of DIPGs;[6,8] however, the occurrence of this substitution in adult thalamic glioma has not been examined. We found that the *H3F3A* K27M mutation was highly prevalent in cases of thalamic GBM in young adults; moreover, this mutation was found in 90% (9/10 cases) of high-grade thalamic gliomas in patients between 20 and 46 years of age. In contrast to *IDH* mutations, the *H3F3A* K27M mutation seemed infrequent in low-grade gliomas; DAs from patients of 29 or 30 years of age did not have the *H3F3A* K27M mutation. For DIPGs, a small number of low-grade astrocytomas were reported to have the *H3F3A* K27M mutation,[8] but in general the *H3F3A* K27M mutation seemed to be specific to high-grade gliomas.[5,7,18]

H3F3A encodes H3.3, a specialized histone variant. H3.3 is deposited on chromatin in a replication-independent manner and is enriched at actively transcribed genes and heterochromatic regions, such as telomeres and pericentromeric regions.[19] Histone 3 lysine 27 trimethylation (H3K27me3), which is mediated by the histone-methyltransferase enhancer of zeste homolog 2 (EZH2), a member of the Polycomb family, is associated with the silencing of transcription.[20] Reportedly, tumors with the *H3F3A* K27M

mutation have little or no H3K27me3, and they have increased acetylation of H3K27 (H3K27ac); conversely, tumors with wild-type *H3F3A* have increased H3K27me3 and lowered H3K27ac levels.[21,22] Although the mutated histone variant H3.3 accounts for only a small proportion of the entire histone H3 population, reduction of H3K27me3 occurs globally and affects other histone H3 molecules because the K27M peptide reduces the methyltransferase activity of Polycomb repressive complex 2 (PRC2) by inhibiting the catalytic subunit EZH2, which contains a Su(var)3-9/enhancer-of-zeste/trithorax (SET) domain.[22] Moreover, inhibition of PRC2 leads to increased levels of H3K27 acetylation, which is a marker of active enhancers.[23] In fact, gliomas with the *H3F3A* K27M mutation were shown to form a class with a distinctive methylation profile of CpG islands that probably resulted from epigenetic dysregulation.[7] However, the mechanisms by which this dysregulation of histone modification leads to gliomagenesis is unknown. We reasoned that the thalamic gliomas lacking the *H3F3A* mutation might result from a similar mechanism of tumorigenesis as tumors harboring the *H3F3A* K27M mutation; therefore, we performed targeted gene sequencing of molecules that could modulate H3K27 status. The targeted genes included *EZH2*, *KDM6A*, *EP300*, and *CREBBP*. We identified a *KDM6A* mutation (p.R1213L) in one case of DA. This mutation was located in the JmjC domain, and might have similar tumorigenic potential as the *H3F3A* K27M mutation. We also identified a *CREBBP* mutation in a tumor with the *H3F3A* K27M mutation; however, we did not find mutations in any of these genes in the high-grade tumors that lacked the *H3F3A* K27M mutation. Therefore, high-grade thalamic gliomas with wild-type *H3F3A* might have resulted from a tumorigenic mechanism that is not related to H3.3 K27 modifications. However, we did not identify any other driver mutation. Genomic analysis on a larger scale might be required to reveal novel mutations, but thalamic gliomas are rare and biopsy is the standard surgical procedure; therefore, such a large-scale analysis of these gliomas will be difficult.

To further evaluate the molecular characteristics of *H3F3A* K27M-mutant thalamic gliomas, global methylation profiles were examined; the adult thalamic high-grade gliomas with the *H3F3A* K27M mutation had methylation profiles similar to those of *H3F3A* K27M-mutant pediatric glioblastomas. This finding indicated that patient age did not affect the pattern of methylation in K27M-mutant tumors. In contrast, *H3F3A* wild-type adult thalamic high-grade gliomas, which occurred mostly in patients over 50 years of age, shared the molecular characteristics with hemispheric glioblastomas; this finding was expected based on the fact that molecules that could modulate H3K27 status were not mutant in these tumors. These results raised the possibility that treatment strategies in cases of adult glioblastomas should be designed based on tumor location and *H3F3A* mutation status.

In this set of cases, the median overall survivals were only 8.9 months and 15.6 months for patients with GBM and those with AA, respectively. These periods of survival were shorter than the average overall survival among patients with GBM or AA.[24] These gliomas, because of their location, were not amenable to radical tumor resection, and this characteristic might be one reason for the poor outcomes, as the degree of surgical resection is an important prognostic factor.[25] Indeed, diagnostic biopsy was the sole surgical intervention in most of these cases. The absence of *IDH1* and *IDH2* mutations, which were found in ~30% of AA and 10% of GBM in our previous report[16] and are good prognostic markers of longer survival, might also account for the poor prognosis of patients with thalamic gliomas. We also suspected that the low frequency of methylated *MGMT* promoters, which are the key indicators of poor response to temozolomide and are among the most important prognostic factors,[26] might explain the poor survival among younger patients with thalamic glioma who underwent intensive chemoradiotherapy. Indeed, the patients with methylated *MGMT* promoters lived longer than those with unmethylated *MGMT* promoters, but this difference was not statistically significant. In addition, we suspected that *H3F3A* K27M mutation in thalamic gliomas might be associated with poor survival, because *H3F3A* K27M-mutant DIPGs were reportedly associated with worse overall survival than were wild-type tumors.[8] However, in this study, there was no significant difference in overall survival between patients with *H3F3A* K27M-mutant gliomas, which occurred mostly in younger patients, and those with wild-type *H3F3A* gliomas, which occurred mostly in older patients. Nevertheless, our sample size was small, and the prognostic significance of *H3F3A* K27M mutation for thalamic gliomas must be examined further in larger studies.

In conclusion, thalamic gliomas in young adults, as well as those in children and adolescents, often harbor the *H3F3A* K27M mutation. Thalamic high-grade gliomas in young adults may as a group share a particular mechanism of tumorigenesis that is related to the *H3F3A* K27M mutation; therefore, development of customized treatment strategies may be required for this patient population.

Supplementary Material

Supplementary material is available online at Neuro-Oncology (http://neuro-oncology.oxfordjournals.org/).

Funding

This work was supported in part by the National Cancer Center Research and Development Fund (23-A-20), and by Grants-in-Aid for Scientific Research (B) (no. 23390343 to A.M.), Grant-in-Aid for Scientific Research (S) (no. 24221011 to H.A.), Grant-in-Aid for Scientific Research on Innovative Areas (no. 23134501 to A.M.), Grant-in-Aid for Young Scientists (B) (no. 24791486 to K.S.), and a research program of the Project for Development of Innovative Research on Cancer Therapeutics (P-Direct) (A.M., G.N., Y.N., H.A., N.S.) from the Ministry of Education, Culture, Sports, Science, and Technology of Japan. A.M. was also supported by the Takeda Science Foundation and Japan Brain Foundation.

Acknowledgments

The authors thank Reiko Matsuura and Yuko Matsushita for extracting DNA from formalin-fixed, paraffin-embedded samples and blood, Hiroko Meguro for performing the Infinium methylation assays, Kaori Shiina and Saori Kawanabe for gene sequencing, and Ruriko Miyahara for assisting with the analysis of patient information.

Conflict of interest statement. None declared.

References

1. Cheek WR, Taveras JM. Thalamic tumors. *J Neurosurg.* 1966;24(2):505-513.

2. McKissock W, Paine KW. Primary tumours of the thalamus. *Brain*. 1958; 81(1):41–63.
3. Tovi D, Schisano G, Liljeqvist B. Primary tumors of the region of the thalamus. *J Neurosurg*. 1961;18:730–740.
4. Kelly PJ. Stereotactic biopsy and resection of thalamic astrocytomas. *Neurosurgery*. 1989;25(2):185–194.
5. Schwartzentruber J, Korshunov A, Liu XY, et al. Driver mutations in histone H3.3 and chromatin remodelling genes in paediatric glioblastoma. *Nature*. 2012;482(7384):226–231.
6. Wu G, Broniscer A, McEachron TA, et al. Somatic histone H3 alterations in pediatric diffuse intrinsic pontine gliomas and non-brainstem glioblastomas. *Nat Genet*. 2012;44(3):251–253.
7. Sturm D, Witt H, Hovestadt V, et al. Hotspot mutations in *H3F3A* and *IDH1* define distinct epigenetic and biological subgroups of glioblastoma. *Cancer Cell*. 2012;22(4):425–437.
8. Khuong-Quang DA, Buczkowicz P, Rakopoulos P, et al. K27M mutation in histone H3.3 defines clinically and biologically distinct subgroups of pediatric diffuse intrinsic pontine gliomas. *Acta Neuropathol*. 2012; 124(3):439–447.
9. Li H, Durbin R. Fast and accurate short read alignment with Burrows–Wheeler transform. *Bioinformatics*. 2009;25(14):1754–1760.
10. McKenna A, Hanna M, Banks E, et al. The Genome Analysis Toolkit: a MapReduce framework for analyzing next-generation DNA sequencing data. *Genome Res*. 2010;20(9):1297–1303.
11. Wang K, Li M, Hakonarson H. ANNOVAR: functional annotation of genetic variants from high-throughput sequencing data. *Nucleic Acids Res*. 2010;38(16):e164.
12. Robinson JT, Thorvaldsdottir H, Winckler W, et al. Integrative genomics viewer. *Nat Biotechnol*. 2011;29(1):24–26.
13. Esteller M, Sanchez-Cespedes M, Rosell R, Sidransky D, Baylin SB, Herman JG. Detection of aberrant promoter hypermethylation of tumor suppressor genes in serum DNA from non-small cell lung cancer patients. *Cancer Res*. 1999;59(1):67–70.
14. Cancer Genome Atlas Research Network. Comprehensive genomic characterization defines human glioblastoma genes and core pathways. *Nature*. 2008;455(7216):1061–1068.
15. Fontebasso AM, Schwartzentruber J, Khuong-Quang DA, et al. Mutations in *SETD2* and genes affecting histone H3K36 methylation target hemispheric high-grade gliomas. *Acta Neuropathol*. 2013; 125(5):659–669.
16. Mukasa A, Takayanagi S, Saito K, et al. Significance of *IDH* mutations varies with tumor histology, grade, and genetics in Japanese glioma patients. *Cancer Sci*. 2012;103(3):587–592.
17. Fontebasso AM, Liu XY, Sturm D, Jabado N. Chromatin remodeling defects in pediatric and young adult glioblastoma: a tale of a variant histone 3 tail. *Brain Pathol*. 2013;23(2):210–216.
18. Gielen GH, Gessi M, Hammes J, Kramm CM, Waha A, Pietsch T. *H3F3A* K27M mutation in pediatric CNS tumors: a marker for diffuse high-grade astrocytomas. *Am J Clin Pathol*. 2013;139(3):345–349.
19. Goldberg AD, Banaszynski LA, Noh KM, et al. Distinct factors control histone variant H3.3 localization at specific genomic regions. *Cell*. 2010;140(5):678–691.
20. Vastenhouw NL, Schier AF. Bivalent histone modifications in early embryogenesis. *Curr Opin Cell Biol*. 2012;24(3):374–386.
21. Venneti S, Garimella MT, Sullivan LM, et al. Evaluation of histone 3 lysine 27 trimethylation (H3K27me3) and enhancer of zest 2 (EZH2) in pediatric glial and glioneuronal tumors shows decreased H3K27me3 in *H3F3A* K27M mutant glioblastomas. *Brain Pathol*. 2013;23(5): 558–564.
22. Lewis PW, Muller MM, Koletsky MS, et al. Inhibition of PRC2 activity by a gain-of-function H3 mutation found in pediatric glioblastoma. *Science*. 2013;340(6134):857–861.
23. Zhou VW, Goren A, Bernstein BE. Charting histone modifications and the functional organization of mammalian genomes. *Nat Rev Genet*. 2011;12(1):7–18.
24. Shibui S. Report of Brian Tumor Registry of Japan (1984–2000). *Neurol Med Chir (Tokyo)*. 2009;49:1–101.
25. Sanai N, Polley MY, McDermott MW, Parsa AT, Berger MS. An extent of resection threshold for newly diagnosed glioblastomas. *J Neurosurg*. 2011;115(1):3–8.
26. Hegi ME, Diserens AC, Gorlia T, et al. *MGMT* gene silencing and benefit from temozolomide in glioblastoma. *N Engl J Med*. 2005;352(10): 997–1003.

Neurologia medico-chirurgica Advance Publication Date: November 20, 2013

ORIGINAL ARTICLE doi: 10.2176/nmc.oa2012-0441

Toxicity and Outcome of Radiotherapy with Concomitant and Adjuvant Temozolomide in Elderly Patients with Glioblastoma: A Retrospective Study

Kuniaki SAITO,[1] Akitake MUKASA,[1] Yoshitaka NARITA,[2] Yusuke TABEI,[3] Nobusada SHINOURA,[3] Soichiro SHIBUI,[2] and Nobuhito SAITO[1]

[1]*Department of Neurosurgery, The University of Tokyo Hospital, Tokyo;*
[2]*Department of Neurosurgery and Neuro-Oncology, National Cancer Center Hospital, Tokyo;*
[3]*Department of Neurosurgery, Tokyo Metropolitan Cancer and Infectious Diseases Center Komagome Hospital, Tokyo*

Abstract

Radiation therapy with concomitant and adjuvant temozolomide (TMZ) is the standard therapy for nonelderly patients with glioblastoma. However, TMZ-based chemoradiotherapy for elderly patients with glioblastoma is controversial. The aim of this study was to investigate the benefits and adverse effects of this combined therapy in elderly patients with glioblastoma. Of the 76 newly diagnosed glioblastoma patients who were treated with standard radiotherapy (60 Gy/30 fractions) and TMZ, treatment toxicity and therapeutic outcome were evaluated in 27 elderly patients (age 65 years or older) and compared with those of 49 nonelderly counterparts (age younger than 65 years). The incidence of common toxicity criteria Grade 4 adverse events during the concomitant course was higher in the elderly group than that in the nonelderly group (26% versus 8%; p = 0.046). Cognitive dysfunction was observed only in the elderly group (p = 0.042). The median overall survival (OS) and median progression-free survival in the elderly group were 15.2 months (95% confidence interval [CI]; 12.9–18.5) and 8.4 months (95% CI; 5.1–11.7), respectively. OS was significantly shorter in the elderly group than in the nonelderly group (p = 0.021). The recursive partitioning analysis score was a prognostic factor for OS. TMZ-based chemoradiotherapy was associated with an increased risk of Grade 4 adverse events in the elderly patients during concomitant use. Thus, elderly patients who undergo a concomitant course of TMZ must be closely monitored for adverse events. Treatment of glioblastoma in elderly patients must be optimized to reduce toxicity to acceptable levels and to maintain efficacy.

Key words: glioblastoma, elderly, temozolomide, toxicity

Introduction

Glioblastoma multiforme (GBM) is the most common primary brain cancer, and it occurs frequently in elderly people.[1)] The elderly population is growing in many countries; therefore, the number of GBM patients diagnosed at age ≥ 65 years is expected to continue to increase. Despite intensive treatment that could include surgical resection, irradiation, chemotherapy, or some combination of these, patients with GBM have a poor prognosis and a median overall survival (OS) of a little over a year. Moreover, elderly patients are known to have even shorter survival than their younger counterparts.[2)] Based on the findings of a phase III randomized trial, radiotherapy with concomitant and adjuvant temozolomide (TMZ) is considered the standard of care for those patients with GBM who are less than 70 years old.[3)] However, subgroup analysis of this study showed diminishing benefit with increasing age, the hazard ratio being 0.80 for the 66–71 year age group (p = 0.340)[4)]; this finding indicated that combined chemoradiotherapy with this regimen may not represent the optimal approach to treatment of GBM in elderly patients. Therefore, optimization of radiotherapy and chemotherapy for elderly patients with GBM has been an important clinical concern in recent years.

Received December 26, 2012; Accepted April 8, 2013

The decreased survival benefit of TMZ-based chemoradiotherapy in elderly patients might be attributed, in part, to the toxicity of the treatment. Based on data from several reports, elderly patients who undergo the standard 6-week course of radiotherapy with concomitant TMZ chemotherapy suffer adverse events.[5–11] However, the toxicity profile of this combined chemoradiotherapy in elderly patients has not been evaluated thoroughly, particularly in Asian populations. Furthermore, comparisons between adverse events rates in elderly patients and those in younger counterparts have generally not been studied in the setting of ordinary clinical trials. We think that more and better information about the toxicity caused by TMZ-based chemoradiotherapy in elderly patients will help to improve post-operative therapy in this population; therefore, we retrospectively reviewed cases of newly diagnosed GBM that were treated with surgery and TMZ-based chemoradiotherapy in the same institutions during the same period, and we compared the adverse events and therapeutic outcome in elderly patients with those in younger counterparts.

Methods

The authors retrospectively analyzed 76 cases of newly diagnosed GBM that were treated with standard radiotherapy of 60 Gy in 30 fractions with concomitant TMZ-based chemotherapy at the University of Tokyo Hospital, the National Cancer Center Hospital, and Komagome Metropolitan Hospital between October 2004 and April 2010. Of these 76 patients, 27 patients (aged 65 years or older at diagnosis) were classified as elderly, and 49 patients (aged less than 65 years) were classified as nonelderly. The outcome and toxicity of the therapy were compared between these two groups. Patients treated with radiotherapy alone or supportive care were excluded from the analysis. No patient was treated with TMZ alone.

For each case included in the study, radiation therapy started within 2 weeks after surgery, and a total dose of 60 Gy was delivered over 6 weeks on a once-daily schedule of 2.0 Gy per fraction. Concomitant chemotherapy consisted of 75 mg/m^2/day TMZ from the first day of radiotherapy. Adjuvant TMZ was started 4 weeks after the end of radiotherapy and was delivered for 5 days every 28 days. The TMZ dose was 150 mg/m^2 for the first cycle and was increased to 200 mg/m^2 after the second cycle. Patients were closely monitored for toxicity throughout TMZ treatment, and all adverse events were recorded and graded according to the common toxicity criteria (CTC) of the National Cancer Institute, version 4.0. Hematology, complete biochemistry, and other adverse events including disturbance of cognitive function were assessed more than once a week during the concomitant course and once per cycle during the adjuvant course. TMZ was given only if neutrophils were > 1,500/μl and platelets were > 100,000/μl; otherwise, treatment was delayed until adequate recovery. If nadir neutrophil counts < 1,000 μl, nadir platelets counts < 100,000/μl, or a CTC Grade 3 nonhematologic adverse event was observed during adjuvant course, TMZ dose was reduced from 200 mg/m^2 to 150 mg/m^2 or from 150 mg/m^2 to 100 mg/m^2 in subsequent TMZ cycle. TMZ was discontinued in case the treating physician judges to discontinue for any reasons such as disease progression, severe toxicity, patient refusal, and so on. Prophylactic sulfamethoxazole-trimethoprim for *Pneumocystis jiroveci* was given routinely.

Patients were evaluated for response using magnetic resonance imaging neuroimaging, which was performed every two cycles. Tumor progression was defined based on the Macdonald criteria; specifically, the emergence of a new lesion or an increase in tumor size by at least 25% indicated tumor progression.[12]

If a frozen tumor sample from a case was available, a QIAGEN DNA extraction kit was used to extract DNA from the tumor sample. Based on methods described by Esteller et al.,[13] methylation-specific polymerase chain reaction (PCR) following sodium bisulfite DNA modification was used to assess promoter methylation of the O6-methylguanine methyltransferase (*MGMT*) gene. The study was approved by the ethics committee of the University of Tokyo Hospital. All clinical samples were obtained with written informed consent from patients.

The Kaplan-Meier method was used to calculate OS and progression-free survival (PFS), and the log-rank test was used to evaluate differences in progression and in survival in relation to prognostic factors. Comparison of subjects by descriptive or clinical demographical variables was performed by using Fisher's exact test for discrete variables and a Student's *t*-test for continuous variables. The significance level was set at $p < 0.05$. All calculations were performed using JMP version 9 software.

Results

I. Patients' characteristics

Median follow-up periods were not significantly different between the elderly group and the nonelderly group (14.4 months versus 18.9 months; $p = 0.12$). The characteristics of the elderly patients and the nonelderly patients are summarized in Table 1. In

Table 1 Clinical characteristics of elderly and nonelderly patients

	≥ 65 (n = 27)	< 65 (n = 49)	p value
Age (mean ± SD)	71.4 ± 3.8	47.1 ± 2.8	
Sex			
Male	16 (59%)	34 (69%)	0.45
Female	11 (41%)	15 (31%)	
KPS			
< 70	8 (30%)	7 (18%)	0.37
70–100	19 (70%)	31 (82%)	
RPA class			
III		10 (20%)	< 0.0001*
IV	3 (11%)	25 (51%)	
V	21 (78%)	9 (18%)	
VI	3 (11%)	5 (10%)	
Extent of resection			
GTR	6 (22%)	12 (24%)	0.65
PR	16 (59%)	24 (49%)	
Biopsy	5 (19%)	13 (27%)	
MGMT promoter			
Methylated	8 (42%)	12 (41%)	1.0
Unmethylated	11 (58%)	17 (59%)	

*Significant value. GTR: gross total removal, KPS: Karnofsky performance status, *MGMT*: O6-methylguanine methyltransferase, PR: partial removal, RPA: recursive partitioning analysis, SD: standard deviation.

the elderly group, the mean age was 71.4 ± 3.8 years. Of the 27 elderly patients, 16 were male. The Karnofsky performance status (KPS) of the elderly group was under 70 in 8 patients (30%) and 70 or more in 19 patients (70%). According to recursive partitioning analysis (RPA),[14] significantly more patients were classified into poor prognosis group (Classes V and VI) in the elderly group than in the nonelderly group (89% versus 29%; $p < 0.0001$). Methylation-specific PCR was performed in 19 of 27 elderly patients and 29 of 49 nonelderly patients. Among patients with methylation-specific PCR assessment, promoter methylation of *MGMT* was evident in approximately 40% of the patients in both the elderly and nonelderly groups. There were no significant differences between groups as to sex, KPS, extent of resection, or *MGMT* methylation.

II. Toxicity

Adverse events of CTC Grade 3 and 4 that occurred during the concomitant course (Table 2) or the adjuvant course (Table 3) were classified as hematologic or treatment-related nonhematologic. During the concomitant course, lymphocytopenia occurred frequently in both the elderly group (26%) and the nonelderly group (53%). Thrombocytopenia was more frequent in the elderly group than in the nonelderly group ($p = 0.042$); conversely, lymphocytopenia was more common in nonelderly group

Table 2 CTC Grade 3 and 4 adverse events that occurred during the course of TMZ that was administered concomitantly with radiotherapy

	Adverse event	≥ 65 (n = 27)		< 65 (n = 49)		p value
		N	%	N	%	
Hematologic	Leukocytopenia	6 (2)	22 (7)	6 (1)	12 (2)	0.33
	Neutropenia	6 (3)	22 (11)	4	8	0.15
	Lymphocytopenia	7 (3)	26 (11)	26 (3)	53 (6)	0.03*
	Thrombocytopenia	3 (3)	11 (11)	0	0	0.042*
	Overall Grade 3/4	10	37	26	53	0.23
	Overall Grade 4	7	26	4	8	0.046*
Treatment-related nonhematologic	Constipation	0	0	1	2	1.0
	Fatigue	1	4	1	2	1.0
	Pneumonia	1	2	1	2	1.0
	Liver enzyme	3	11	2	4	0.34
	Hypoalbuminemia	1	4	0	0	0.35
	Rash	0	0	1	2	1.0
	Meningitis	1	4	0	0	0.35
	Cognitive dysfunction	3	11	0	0	0.042*
	Overall Grade 3/4	8	30	6	12	0.072

*Significant value. Figures in parentheses show the number or percentage of Grade 4 adverse events. CTC: common toxicity criteria, TMZ: temozolomide.

Table 3 CTC Grade 3 and 4 adverse events that occurred during the course of adjuvant TMZ that was administered after radiotherapy

	Adverse event	≥ 65 (n = 22)		< 65 (n = 45)		p value
		N	%	N	%	
Hematologic	Leukocytopenia	1	5	9 (2)	20 (4)	0.15
	Neutropenia	1	5	2	4	1.0
	Lymphocytopenia	6 (2)	27 (5)	18 (2)	40 (4)	0.42
	Thrombocytopenia	1	5	2 (2)	4 (4)	1.0
	Overall Grade 3/4	8	36	20	44	0.6
	Overall Grade 4	2	9	3	7	1.0
Treatment-related nonhematologic	Nausea	0	0	1	2	1.0
	Anorexia	0	0	1	2	1.0
	Fatigue	1	5	0	0	0.33
	Pneumonia	3	14	2	4	0.32
	Liver enzyme	2	9	4	9	1.0
	Rash	1	5	2	4	1.0
	DVT/PE	0	0	1	2	1.0
	Cognitive dysfunction	1	5	0	0	0.33
	Viral infection	0	0	2	4	1.0
	Overall Grade 3/4	8	36	10	22	0.25

Figures in parentheses show the number or percentage of Grade 4 adverse events. CTC: common toxicity criteria, DVT: deep vein thrombosis, PE: pulmonary embolism, TMZ: temozolomide.

(p = 0.03). Although the incidence of overall Grade 3 and 4 adverse events was similar in both groups, more patients in the elderly group suffered Grade 4 hematological adverse events than did those in the nonelderly group (26% versus 8%; p = 0.046). Total 12 Grade 4 hematologic adverse events (leukocytopenia, 2; neutropenia, 3; lymphocytopenia, 4; thrombocytopenia, 3) were observed during the concomitant course in seven elderly patients. Two of 7 (29%) elderly patients with Grade 4 hematological adverse event could not start the adjuvant TMZ course because of prolonged myelosuppression. With respect to nonhematologic toxicity, cognitive dysfunction was observed in three elderly patients during concomitant course, while it was not observed in nonelderly patients (p = 0.042).

During the adjuvant course of TMZ, 4 of 22 elderly patients (18%) and 2 of 45 nonelderly patients (4.4%) required dose reduction (p = 0.46). The frequency of overall Grade 3 and 4 adverse events was comparable between the two groups. Grade 4 adverse events occurred in 9% of the elderly group and in 7% of the nonelderly group (p = 1.0) during the adjuvant course of TMZ.

III. TMZ cycle number and interval

The number and interval of TMZ cycles are shown in Table 4. The mean number of adjuvant cycles of TMZ was 4 in the elderly and 6.3 in the nonelderly. The mean number and the interval of adjuvant cycles were not significantly different between the two groups (p = 0.066 and 0.69, respectively), while the duration between the last day of the concomitant course and the first adjuvant cycle was significantly longer in the elderly group (48.4 versus 34.5 days; p = 0.01). Reasons for discontinuation of the adjuvant course included recurrence, deterioration of performance status, severe adverse effect, and patient refusal.

Table 4 Number and interval of TMZ cycles

	≥ 65	< 65	p value
Numbers of TMZ cycle	4.0 ± 2.0	6.3 ± 1.5	0.066
Interval of TMZ cycle (days)	32.4 ± 2.5	31.8 ± 1.67	0.69
Interval between concomitant TMZ and adjuvant TMZ (days)	48.4 ± 8.8	34.5 ± 5.9	0.01*

*Significant value. Each number indicates mean ± standard deviation. TMZ: temozolomide.

IV. OS and PFS

Figure 1 shows the Kaplan-Meier analysis for OS and PFS of the patients in the elderly and nonelderly groups. The median OS was 15.2 (95%

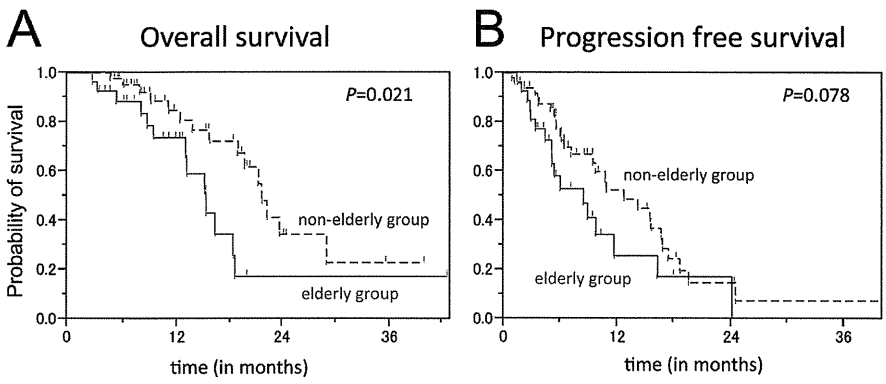

Fig. 1 Kaplan-Meier analysis for (A) overall survival and (B) progression-free survival of the patients in the elderly group and the nonelderly group.

confidence interval [CI]; 12.9–18.5) months in the elderly group and 21.6 (95% CI; 18.0–29.0) months in the nonelderly group. OS was significantly longer in the nonelderly group (log-rank test, p = 0.021).

PFS was 8.4 (95% CI; 5.1–11.7) months in the elderly group, and 12.7 (95% CI 9.5–16.7) months in the nonelderly group (p = 0.078); PFS tended to be longer in the nonelderly group.

V. Prognostic factors and effect on OS and PFS in the elderly group

Results of univariate analysis of prognostic factors are shown in Table 5. RPA score (IV and V versus VI; p < 0.01) was the prognostic factors for OS. Median OS was 15.1 months in the age 65–69 bracket, 18.5 months in the age 70–74 bracket, and 15.3 months in the age 75-years-and-over bracket.

RPA score (IV and V versus VI) seemed to be a prognostic factor for PFS with borderline significance (p = 0.05). Extent of resection (gross total removal versus partial removal and biopsy), KPS, and *MGMT* promoter methylation were poorly correlated with PFS. Median PFS was 5.3 months in the age 65–69 bracket, 9.8 months in the age 70–74 bracket, and 8.9 months in the age 75-years-and-over bracket. Like OS, PFS did not differ significantly between the age brackets within the elderly group.

Table 5 Prognostic factors for OS and PFS

	N	Median OS (months)	p value	Median PFS (months)	p value
Sex					
Male	16	15.1	0.83	6	0.93
Female	11	16.2		8.9	
Age					
≥ 75	7	15.3	0.72	8.9	0.41
70–74	11	18.5		9.8	
65–70	9	15.1		5.3	
Extent of resection					
GTR	6	n.r.	0.57	8.9	0.31
PR, biopsy	21	15.1		6	
KPS					
≥ 70	19	15.3	0.63	8.4	0.95
< 70	8	12.9		9.8	
RPA score					
IV–V	24	16.2	< 0.01*	8.9	0.05
VI	3	9.3		3.4	
MGMT					
Methylated	8	12.9	0.7	5.3	0.33
Unmethylated	11	18.5		9.8	
Adverse event (Grade 4)					
(+)	8	15	0.15	8.4	0.75
(–)	19	15.3		8.9	

*Significant value. GTR: gross total removal, KPS: Karnofsky performance status, *MGMT*: O6-methylguanine methyltransferase, n.r.: not reached, OS: overall survival, PFS: progression-free survival, PR: partial removal, RPA: recursive partitioning analysis.

Discussion

In this study, an increased incidence of Grade 4 adverse events and cognitive dysfunction was observed in the elderly patients especially during the concomitant course. Overall Grade 3 and 4 hematologic toxicity during concomitant and adjuvant chemotherapy with TMZ in the elderly patients was reported to range from 6% to 18% and 10% to 22%, respectively.[5,6,9,10] Meanwhile, the present study showed a higher incidence of overall Grade 3 and 4 hematologic toxicity in elderly patients; 37% and 36% during the concomitant and adjuvant courses, respectively. Unexpectedly, this higher rate of hematologic toxicity was not specific to elderly patients, and the incidence of overall Grade 3 and 4 hematologic toxicity in the nonelderly group was

53% and 44% during the concomitant and adjuvant courses, respectively. Although the reasons for the high hematologic toxicity rates in the nonelderly and the elderly patients in the present study were not evident, most of these toxicity seemed not to have affected the schedule of TMZ administration because much of Grade 3 and 4 hematologic toxicity that we recorded was lymphocytopenia without severe infectious disease. On the other hand, the incidence of Grade 4 toxicity that caused discontinuation or delay of TMZ administration was significantly higher in the elderly than in the nonelderly patients, and such Grade 4 toxicity was mostly observed during concomitant course; these findings indicated that there was a potential risk in treating elderly patients with TMZ in this fashion.

Besides hematologic toxicity, it is noteworthy that cognitive dysfunction was found only in elderly patients; this adverse event occurred in 11% of elderly patients during the concomitant course and in 5% during the adjuvant course. Cognitive dysfunctions were observed ahead of disease progression, and median time to onset of cognitive dysfunction was 1 month, while median time to progression of these patients was 11.7 months. So we think these cognitive dysfunctions were not caused by disease progression. As Brandes et al. reported mental status deterioration during adjuvant TMZ chemotherapy after concomitant chemoradiotherapy in 56% of elderly patients,[6] neurotoxicity is a common finding in elderly patients. In contrast to the report from Brandes et al.,[6] we observed a higher frequency of cognitive dysfunction during concomitant course of TMZ in the elderly. Thus, the cognitive function of elderly patients should be monitored carefully. However, the causal association between cognitive dysfunction and TMZ was unclear because there were many causes for cognitive dysfunction other than TMZ, such as aging and radiotherapy itself; a controlled study is required to evaluate the causes of cognitive dysfunction in elderly patients with GBM.

In contrast to during the concomitant course, the incidence of Grade 3 and 4 adverse events during the adjuvant course did not differ significantly between the elderly group and the nonelderly group. The mean interval of each adjuvant cycle was also similar between the two groups (32.4 versus 31.8; $p = 0.69$). Therefore, the elderly patients seemed to tolerate the adjuvant course as well as the younger patients did. The reason why severe adverse events happen more frequently during concomitant course is unclear; however, one hypothesis is that a higher accumulated dose of TMZ within a course of chemotherapy tends to cause severe toxicity in elderly patients who have relatively poor tolerance potential to chemotherapy including bone marrow function than the younger. Indeed, in this treatment regimen, patients were scheduled to receive 6 weeks of continuous administration of TMZ in concordance with 60 Gy radiation, which amounts to over 3,000 mg/m^2 of TMZ. On the other hand, during a cycle of adjuvant course, patients were administered with only 750–1,000 mg/m^2 of TMZ with 23 days cessation period. If this explanation is true, a reduction of the TMZ dose or a shortening of administration period of TMZ during the concomitant course might decrease the rates of complications, although these changes may also cause a reduction in therapeutic effect because concomitant course is theoretically the most active portion of the TMZ-based chemoradiotherapy regimen.

The median OS and the median PFS in the elderly group were 15.2 and 8.4 months, respectively, in this study. Brandes et al. recently reported median OS of 13.7 months and PFS of 9.5 months in 58 patients with GBM who were 65 years of age or older and were treated with concomitant and adjuvant TMZ added to standard radiotherapy.[6] Minniti et al. also reported a median OS of 12.8 months and a median PFS of 7.5 months in a study of 83 patients 70 years of age or older who received standard radiotherapy plus concomitant and adjuvant TMZ.[15] The present results compare favorably with these reports. Notably, patients aged 75 years and older (7/27 patients; 26%) had no worse outcomes than did those of 65–74 years; the median OS and median PFS were 15.3 and 8.9 months in patients aged 75 years and older, 18.5 and 9.8 months in the 70–74 year group, and 15.1 and 5.3 in the 65–70 year group. Baseline KPS ranged from 50 to 90 with median KPS of 80 in patients aged 75 years or older and from 60 to 90 with median KPS of 80 in the 65–74 year group. These facts make it difficult to set an age-based cut-off line for determining who should be treated as the elderly patient. In this analysis, we categorized the patients older than 65 years as the elderly as have other research groups[6,9,16,17] and does the ongoing randomized clinical trial (NCIC/EORTC 26062).

Several important findings on the optimal treatment of the elderly patients with GBM have been reported recently. Findings from randomized controlled trials demonstrated (1) that radiotherapy alone (60 Gy/30 fractions) could prolong survival more than the best supportive care could and radiotherapy did not compromise quality of life or cognition[18] and (2) that an abbreviated course of radiotherapy (40 Gy/15 fractions) was equivalent to standard radiotherapy of 60 Gy over 30 fractions in the elderly GBM patients.[19] Thus, considering the